Contents lists available at ScienceDirect

Applied Catalysis B: Environmental

Review

Photocatalytic oxidation technology for indoor environment air purification: The state-of-the-art

Alireza Haghighat Mamaghani, Fariborz Haghighat*, Chang-Seo Lee

Department of Building, Civil and Environmental Engineering, Concordia University, Montreal, Canada

ABSTRACT

Inevitable presence of volatile organic compounds (VOCs) in indoor environment and their adverse impact on human health and productivity have encouraged the development of various technologies for air pollution remediation. Among these technologies, photocatalytic oxidation (PCO) is regarded as one of the most promising methods and has been the focus of many research works in the last two decades. Titanium dioxide (TiO$_2$) is by far the most investigated photocatalyst for photocatalytic degradation of gaseous VOCs. This review article is intended to provide a comprehensive overview of the application of commercial TiO$_2$ photocatalysts for removal of VOCs in air. First, the fundamentals of photocatalytic oxidation are briefly discussed and common TiO$_2$-based photocatalysts are introduced. Then, the relations between the characteristics of photocatalysts (e.g. crystallinity, surface area and surface chemistry) and photocatalytic activity as well as the influence of key operating parameters on PCO processes are investigated. Afterwards, the reaction mechanisms and identified reaction intermediates/by-products for the most prevalent VOC families are reviewed. Finally, the paper discusses the deactivation of photocatalysts during PCO processes and some of the common regeneration techniques.

© 2016 Elsevier B.V. All rights reserved.
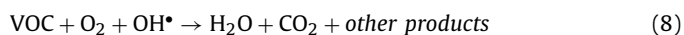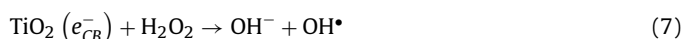
Contents

* Corresponding author.
E-mail addresses: alireza.haghighat@mail.polimi.it (A.H. Mamaghani), fariborz.haghighat@concordia.ca (F. Haghighat), chang-seo.lee@concordia.ca (C.-S. Lee).

1. Introduction

Owing to the fact that nowadays people spend most of their time (more than 90% [1]) in an indoor environment, indoor air quality (IAQ) has a significant impact on human health, comfort and productivity [2]. A long-term exposure to indoor air pollutants can be detrimental to human health and lead to sick building syndrome, building related illnesses and in extreme cases cancer [3]. VOCs, nitrogen oxides (NO$_x$), carbon monoxide (CO), and particulate matter are among the main indoor air pollutants. Levels of pollutants in indoor environment can be higher than that of outdoor air due to the contribution of indoor sources such as combustion by-products, building materials, office equipment (e.g. printers and computers), and consumer products [3,4]. VOCs mainly contain alkanes, aromatics, esters, alkenes, carboxylic acids and alcohols [2]. Considering the growing concerns regarding the IAQ, many technologies have been developed for removing VOCs from indoor air such as adsorption [5–8], ozonation [9–11], non-thermal plasma [12,13], and photocatalytic oxidation [14–17].

In the last two decades, PCO technology has attracted great attention for removal of gaseous pollutants at low concentrations (i.e. part per billion (ppb) level), owed to its superior features such as room temperature operation, activity towards various contaminants, and benign final products (CO$_2$ and H$_2$O). PCO technology is basically founded on the application of semiconductor catalysts, such as TiO$_2$, and ultraviolet (UV) light to convert challenge compounds into less harmful products. In PCO, a crucial step is the formation of electron and hole (e$^-$-h$^+$) pairs which requires the illumination of semiconductor, absorption of photons with sufficient energy, and promotion of electrons from the valence band to the conduction band [18]. The photogenerated charge carriers participate in a series of reactions with other molecules such as oxygen and water and produce highly reactive radicals (such as hydroxyl radical). In gas phase PCO, mass transfer of the VOC compounds from the gas phase (i.e. air stream) to the solid phase plays an important role and greatly affects the reaction rate and removal efficiency. After the external (from bulk to exterior surface) and internal diffusions (from exterior surface to internal catalytic surface) and adsorption onto the surface, pollutant molecules come into contact with the produced reactive species and break down to lower molecular weight products and eventually to CO$_2$, water and other by-products [2,19]. The basic PCO reaction mechanism using TiO$_2$ can be depicted as follows:

$$TiO_2 + h\nu \rightarrow TiO_2(e^-_{CB} + h^+_{VB}) \tag{1}$$

$$TiO_2(h^+_{VB}) + H_2O \rightarrow TiO_2 + H^+OH^\bullet \tag{2}$$

$$TiO_2(h^+_{VB}) + OH^- \rightarrow TiO_2 + OH^\bullet \tag{3}$$

$$TiO_2(e^+_{CB}) + O_2 \rightarrow TiO_2 + O^{\bullet-}_2 \tag{4}$$

$$O^{\bullet-}_2 + H^+ \rightarrow H^\bullet_2 \tag{5}$$

$$HO^\bullet_2 + HO^\bullet_2 \rightarrow H_2O_2 + O_2 \tag{6}$$

$$TiO_2\left(e^-_{CB}\right) + H_2O_2 \rightarrow OH^- + OH^\bullet \tag{7}$$

$$VOC + O_2 + OH^\bullet \rightarrow H_2O + CO_2 + other\ products \tag{8}$$

Apart from their beneficial participation in oxidation and reduction reactions, electrons and holes also go through recombination process where they neutralize one another. The recombination of charge carriers, whether in the bulk or on the surface, drastically decreases the quantum efficiency and accordingly the PCO performance [20].

Among a wide spectrum of photocatalysts (e.g. TiO$_2$, ZnO, ZrO$_2$, SnO$_2$, WO$_3$, CeO$_2$, ZnS, and Fe$_2$O$_3$), TiO$_2$, as the most promising photocatalyst, has been the focus of majority of the works owing to

its moderate performance as a photocatalyst under UV light irradiation, chemical stability, and suitable positions of valence and conduction bands [21]. To date, numerous TiO$_2$ photocatalysts with different morphological designs have been developed: nanoparticles, nanotubes, hollow fibers, and mesoporous [4,22]. As one can note by the number of publications in the past 15 years, there is great interest in the application of commercial photocatalysts for the removal of VOCs from air. To this end, extensive research efforts have been devoted to evaluate the performance of several commercially available photocatalysts for such application. TiO$_2$ Aeroxide P25 from Evonik® is by far the most employed photocatalyst in this field owing to its high performance in degradation of many VOCs, availability, and relatively low cost [23]. The other common commercial titanium dioxides are PC series (Cristal Global Companies), Hombicat® UV100, and Aerolyst 7710 (Evonik®) [24–27]. Table 1 summarizes some of the key characteristics of different commercial photocatalysts.

In most of the published articles, limited explanations were provided to enable the reader make connections between the morphology, electronic properties, and surface chemistry of the photocatalyst and the obtained photocatalytic activity toward a specific VOC. It is believed that a comprehensive review of TiO$_2$ photocatalysts, specifically applied in the PCO of indoor air pollutants, would provide more insight into the crucial characteristics needed in an efficient and long-lasting photocatalyst.

2. Photocatalyst characteristics

Photocatalytic performance of TiO$_2$ depends on several factors including crystallinity, crystalline phase, crystal size, accessible surface area, pore structure, pore size, and adsorption capacity [33,34]. Depending on the target VOC and the main operating parameters, the abovementioned properties can affect the photocatalytic activity to different extents.

2.1. Effect of photocatalyst crystallinity and crystal size

Light harvesting, charge carrier generation (i.e. electron excitation) and separation, and charge migration to the surface exert significant influence on the quantum efficiency and photocatalytic activity of TiO$_2$. Due to the fact that recombination process is facilitated by the presence of lattice defects, crystal imperfections and impurities, much attention has been paid to the achievement of high bulk crystallinity in order to enhance the photon utilization efficiency [35]. Anatase and rutile are the main crystalline structures of TiO$_2$ with energy band-gaps of 3.23 and 3.02 eV, respectively [36]. It is generally recognized that anatase is more active than rutile, which can be ascribed to several properties of anatase phase: (i) better generation of e$^-$-h$^+$ pair; (ii) higher affinity towards O$_2$ due to the more negative redox potential of conduction band; (iii) higher amount of surface hydroxyl groups which improve chemisorption properties; and (iv) lower recombination rate than rutile [4,33].

In the case of P25, it seems that the source of its high photocatalytic activity is still a matter of debate [23]. It has been suggested that due to the co-presence of anatase and rutile phases, e$^-$-h$^+$ can transfer between interconnecting anatase and rutile particles and prevent charge recombination [37,38]. Ohno et al. [39] attributed the high photocatalytic activity of P25 to the band bending in rutile particles which are in contact with anatase particles. On the other hand, Bickley et al. [40] proposed that the key reason for P25 high activity is the presence of particles made of anatase nuclei inside a rutile layer which elongates the e$^-$-h$^+$ lifetime (e$^-$ in anatase and h$^+$ in rutile). Some studies have employed time resolved microwave conductivity (TRMC) to study the charge carrier trans-

Table 1
Characteristics of several commercial photocatalysts [25–32].

Photocatalyst	Properties					
	BET (m^2/g)	Crystal size (nm)	Band gap (eV)	Mean pore radius (nm)	Crystalline phase	Other remarks
P25	47	25.8	3.01	–	Anatase (80%) and Rutile (20%)	Non-porous material with interparticle pores (meso and macropore)
PC500	276	12.9	3.14	6.1	Anatase	Type IV sorption isotherms indicates the presence of mesopores
PC105	80	23	3.19	15.3	Anatase	–
PC100	90	15	–	–	Anatase	–
UV100	330	<10	3.1	<5	Anatase	Agglomeration of small subparticles into round-shaped particles generates high density small pores with characteristic of microporous materials
Aerolyst 7710	53	25	–	30–40	Anatase (82%) and Rutile (18%)	–

fer in semiconductors [41,42]. Hajaghazadeh et al. [30] ascribed the higher initial mineralization rate of methyl ethyl ketone (MEK) over P25 and PC50 compared to that of PC500 to the slow decay of charge carriers in P25 and PC50, which was also reported by other researchers using TRMC [41,42]. Similar behavior has been reported by Thevenet et al. [43] in acetylene degradation over P25 and PC500; however, the superior activity of P25 was rationalized differently. The authors speculated that since P25 particles are single crystallites, the electron migration to the surface is easier/faster than in PC500 where electrons have to cross crystallites interfaces. On the other hand, it should be noted that PC500 is synthesized hydrothermally under low calcination temperatures and consequently possesses larger number of defect sites, resulting in higher recombination rate. Taranto et al. [32] claimed that higher initial reaction rate of *n*-octane over P25 and PC105 compared to PC500, despite their lower surface areas, could arise from their preparation methods at high temperatures which led to lower structural defects.

Besides crystallinity, several authors have stressed the critical role of crystal size in PCO reactions in the gas phase. It has been proposed that small particle size of UV100 (~10 nm) results in a better balance between surface and bulk recombination [26,44]. Alonso-Tellez et al. [26] argued that this feature of UV100 is the key reason for its superior performance in comparison to P25 in photocatalytic oxidation of MEK. Furthermore, it was observed that nano-sized photocatalysts, P25 and PC105, exhibit higher performance in degradation of acetone, acetaldehyde, and toluene with respect to the micro-sized ones, Kronos 1077 and Cristal AT-1 [28].

Based on the reported results, it can be concluded that higher crystallinity, smaller crystal size, and co-presence of anatase and rutile might bring about higher reaction rate; notwithstanding, there are examples where these trends have not been necessarily followed [33,45,46].

2.2. Effect of catalyst surface area, porosity, and surface chemistry

The photocatalytic activity can be greatly influenced by the structural features such as surface area and porosity. Keeping the surface chemistry unchanged, as the surface area is increased, greater numbers of active sites and e^--h^+ pairs and higher concentration of pollutants on the photocatalyst can be envisaged. In view of this, larger surface area can enhance the photocatalytic activity and mineralization of challenge compounds to CO_2 [26].

Hajaghazadeh et al. [30] reported that MEK conversion follows the order of PC500 > P25 > PC50 under steady state condition. It was suggested that PC50 and P25 activities drop over time because

of their low surface areas while for PC500 the positive impact of high surface area outweighs the adverse effect of fast e^--h^+ recombination in long-term. Similar trends have been observed by Taranto et al. [32] in PCO of methanol where initially P25 and PC105 outperform PC500 owing to their lower charge carriers decay; however after 45 min, PC500 performs better in terms of conversion and mineralization since high surface area of PC500 allows higher adsorption of methanol and formaldehyde (methanol PCO intermediate). The greater influence of surface area on pollutant conversion with regard to crystallinity has also been noted in degradation of perchloroethylene (PCE) over P25 and PC500 [37].

Alonso-Tellez et al. [26] pointed out that, apart from its higher surface area, one of the major reasons for superior photocatalytic activity of UV100 compared with P25 is its microporosity. They underlined that small pores of UV100 can retard the escape of pollutants from photocatalytic coating (i.e. increasing the residence time) and increase the probability of reactants adsorption and reaction on the surface. In addition, an interconnected pore system, such as in UV100, can facilitate the diffusion of reactants towards active sites and enhance light harvesting. Suligoj et al. [27] attributed the fast PCO reaction of formaldehyde over PC500 to the presence of mesopores (2.1 nm) which enable the access of small molecules like formaldehyde and improve the adsorption.

It should be noted that besides surface area and porosity, surface chemistry can also play a critical role in gas phase PCO reactions [46,47]. Verbruggen et al. [47] estimated that the effective surface area available for acetaldehyde adsorption on PC500 is 3.5 times higher than P25, while, interestingly, PC500 BET (Brunauer–Emmett–Teller) surface area is about six times than that of P25. They justified that the adsorbed amount of acetaldehyde agrees well with the total number of OH groups (obtained from thermogravimetric measurements (TGA)) on PC500 surface which is nearly four times of that on P25. Bianchi et al. [28] highlighted that the abundance of surface hydroxyl groups on PC105 is the key to its high photocatalytic activity. Using Fourier transform infrared spectroscopy (FTIR), they showed that among different types of OH reactive sites on P25 and PC105 (e.g. H-bonded OH, terminal Ti–OH, and Ti–OH–Ti bridged), Ti–OH–Ti bridged species were the most influential groups in the PCO of acetone and acetaldehyde. d'Hennezel et al. [48] found that water-impregnation and HCl-impregnation of P25 can improve the PCO of benzene and toluene owing to the higher amount of hydroxyl groups on TiO_2/H_2O and the chlorine radical chain transfer mechanism over TiO_2/HCl. In another study, in order to determine the presence of Lewis or Bronsted acid centres on P25, PC100, and UV100, Arana et al. [46] investigated the interaction of ammonia with the catalysts sur-

face. The FTIR spectra of NH_3 interaction with these photocatalysts revealed the presence of both acid centres, Lewis and Bronsted, with the following intensity: P25 > UV100 > PC100.

One of the well-established techniques to alter photocatalyst crystallinity and structural properties is heat treatment. Heat treatment of catalyst at high temperatures on the one hand improves the crystallinity (i.e. less bulk defects), whereas on the other hand it adversely affects the surface area and porous structure [33,34,49]. Kirchnerova et al. [31] investigated the impact of thermal treatment on P25 and UV100 characteristics and photocatalytic activity. It was observed that short time calcinations at 623 K and 973 K bring about crystal growth, sharp decline in surface area, and quasi permanent elimination of hydroxyl groups for both P25 and UV100. In addition, they observed that the heat treatment had a negative impact on *n*-butanol adsorption on P25 and UV100 due to the loss of surface area and surface hydroxyl groups; while higher *n*-butanol conversion was achieved on calcined UV100 probably because of improved crystallinity after high temperature calcination [31]. Yu et al. [50] reported that the photocatalytic activity of P25 towards acetone oxidation improves by thermal treatment at temperatures up to 400 °C and decreases at higher temperatures due to the formation of rutile phase. The authors stated that the thermally treated TiO_2 shows superior ability in adsorbing oxygen on its surface which results in generation of superoxide anion radicals under UV irradiation and better separation of e^--h^+.

On condition that high surface area, porous structure, and large amount of surface hydroxyl groups (and other surface reactive species) can be achieved without substantial loss of crystallinity, the prevailing view is that these features can be of greater importance compared to crystallinity in long-term.

2.3. Effect of catalyst surface density

Taking into account that most of the commercial photocatalysts are in the form of nanoparticle powder, different coating techniques have been employed for catalyst immobilization on support material [21]. Dip-coating is the most popular method in the laboratory scale and has been applied for deposition of commercial photocatalysts on different substrate materials (e.g. glass plate, fiber glass, and activated carbon (AC)) [32]. In order to acquire more information about photocatalyst properties and assess the quality of coating, various characterization techniques including scanning electron microscope (SEM), transition electron microscope (TEM), X-ray diffraction (XRD) and nitrogen adsorption-desorption isotherms are utilized [51].

Photocatalyst loading (i.e. catalyst surface density) on support material is an important factor since it directly alters the available surface area and the number of TiO_2 active sites. Increasing the catalyst layer thickness results in higher surface area, lower adsorption competition between reactants and consequently higher removal rate and mineralization degree, especially in short residence times [52]. Nevertheless, it is worth mentioning that considering the coverage rate of photocatalyst on the support material would be a better measure of the portion of photocatalyst which can be activated by light and also is accessible to the pollutants [53,54].

For instance, as the number of coating increased from 2 to 6, toluene conversion gradually improved from 26% to 43% [51]. Similar behavior, constant increase in VOC conversion with catalyst loading, has been observed in photocatalytic oxidation of benzene over P25 [55], 2-propanol over PC500 [56], and ethylene over Aerolyst 7710 [29]. On the other hand, some studies claimed that excessive TiO_2 particle concentration can mask part of the catalytic bed (also known as the screening effect) and counterbalance the advantageous effect of higher photocatalyst mass on support. In this regard, it has been observed that under UVA irradiation, MEK conversion increased with photocatalyst loading until
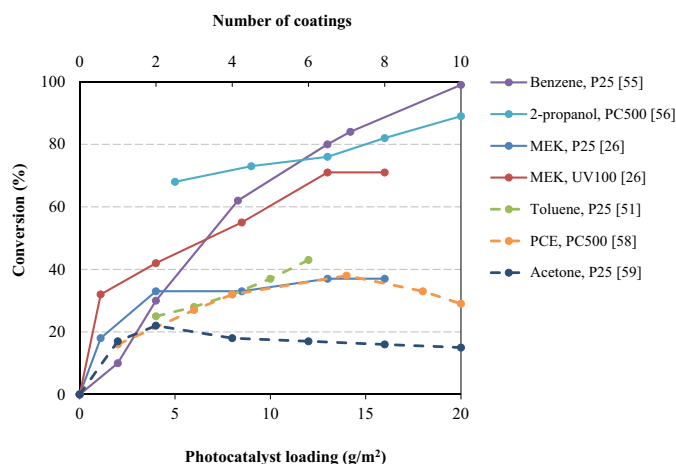

Fig. 1. Effect of photocatalyst loading on VOC removal efficiency; dashed lines: conversion vs number of coatings and solid lines: conversion vs photocatalyst loading (g/m^2).

it reached its plateau: 72% over UV100 at 13 g/m^2 and 38% over P25 at 7 g/m^2 [26]. This trend was attributed to the trade-off between higher surface area and unfavorable screening effect at higher catalyst loadings. Jacoby et al. [57] suggested that trichloroethylene (TCE) reaction rate increased with film loading up to 5 g/m^2 and additional film loading contributed nothing to the photocatalytic efficiency. It is also important to bear in mind that multiple coatings of the same substrate means several heating cycles of photocatalyst which may lead to a decrement in the porosity of photocatalytic film [52]. Some studies stated that there could be an optimum number of coating layers after which removal rate declines [52,58,59]. For instance, Monteiro et al. [58] observed that PCE conversion over PC500 improves with increasing the number of coating up to seven and decreases afterwards. They argued that thicker coating may create "shadowed" areas where no e^--h^+ pair is generated and, consequently, no pollutant molecules are oxidized. Employing 254 + 185 nm UV irradiation, Quici et al. [52] observed that toluene conversion peaks at film thickness of 500 nm where catalyst is effectively irradiated and diffusion of molecules through the porous media is not retarded. Fig. 1 depicts the effect of photocatalyst loading on the removal efficiency of several VOCs over different commercial TiO_2 photocatalysts. As can be seen, in the majority of studies increasing the photocatalyst loading (or the number of coating layers) has substantially improved the VOC conversion while in some cases small decrements in conversion resulted from excessive photocatalyst loading.

2.4. Effect of photocatalyst adsorption properties

Adsorption of pollutant onto the surface of photocatalyst is a crucial step that greatly affects the reaction rate and removal efficiency. Adsorption of challenge compounds on photocatalyst brings about better contact between photocatalyst and reactant molecules, which in turn leads to higher oxidation rate. The role of adsorption step is more critical when dealing with gas streams with high humidity level (typical condition in the mechanical ventilation system of buildings) due to the competition between VOC and water molecules for adsorption sites.

Depending on the type of active site available on the surface of photocatalyst and target VOC, different adsorption mechanisms may exist. Nimlos et al. [60] suggested that alcohols and organic acids can be adsorbed over the surface of TiO_2 via both dissociative adsorption at oxygen bridging sites and hydrogen bond to the OH groups while aldehydes can only be adsorbed via hydrogen bond to the surface OH groups. Based the obtained adsorption efficiencies

for several linear and branched alkanes (pentane < hexane < *i*-pentane < *i*-hexane < heptane), Boulamanti and Philippopoulos [61] reported that branched molecules are more strongly adsorbed on P25. Given the similarities in molecular structure, it was suggested that toluene, *m*-xylene, and *p*-xylene can be adsorbed on P25 via the OH. . .π electron-type interaction, and accordingly, adsorption competition among them is expected [62]. In a detailed study on PCO of aromatics [63], it was shown that the adsorption constants follow the sequence: ethylbenzene < benzene < *o*-xylene < *p*-xylene ∼ *m*-xylene ∼toluene. The authors highlighted that the low adsorption of ethylbenzene and *o*-xylene could result from their molecular structures which induce bigger stereochemical hindrance during adsorption on P25. Qijin et al. [64] examined the adsorption of methanol−benzene binary mixture over P25 in a fluidized bed reactor and argued that due to the presence of electron-donor functional group, hydroxy group, in methanol the adsorption affinity of methanol is stronger than that of benzene (resulting from van der Waals forces). Similarly, Alberici and Jardim [65] reported that the adsorption of VOCs on P25 follows the order: methanol > isopropanol > MEK > acetone > toluene > *i*-octane, indicating higher adsorption of alcohols than aromatics over TiO$_2$. Based on the FTIR spectra of P25 and PC500 in contact with acetaldehyde, Verbruggen et al. [47] concluded that on P25 acetaldehyde adsorbs via H-bridge with a surface hydroxyl group (CH$_3$CH=O$\cdots$HO−Ti) and carbonyl bonding with a cation Ti^{4+} surface group (CH$_3$CH=O$\cdots$Ti^{4+}); while on PC500, acetaldehyde mainly binds with the surface hydroxyl groups. Suligoj et al. [27] reported that toluene adsorption (defined as $100 \times (C_{Toluene,0} - C_{Toluene,t})/C_{Toluene,0}$) over P25 is slightly higher than that over PC500 (12.6% vs 7.1%), while in the case of formaldehyde, PC500 considerably outperforms P25 (75.6% vs 9.8%). Interestingly, Kirchnerova et al. [31] suggested that lower PCO of *n*-butanol over UV100 with regard to P25 is due to the fact that high adsorption capacity of UV100 (about four times higher than that of P25) inhibits the progress of PCO reactions.

The influence of humidity on PCO performance is discussed in detail in section 3.3; consequently, the main focus here is on the role of humidity content in the adsorption of VOCs/intermediates. Based on a competition mechanistic approach, an increment in humidity lowers the ratio of free adsorption sites to pollutants which subsequently reduces the adsorption efficiency. In this regard, Vildozo et al. [66] demonstrated that under dry condition, there is no adsorption competition between 2-propanol (250 ppb) and toluene (80 ppb) for active sites on PC500; however, at RH = 60%, dark adsorptions of 2-propanol and toluene respectively decreased by 30% and 50% compared to the dry condition. In a study on the competitive interaction between water and different VOCs, Yu et al. [67] noted a positive linear relationship between the reciprocal of Langmuir adsorption constant and the Henry's Law constant of aromatic compounds. Geng et al. [68] and Zhang et al. [69] noticed a significant decrease in cyclohexane and chlorobenzene adsorption with increasing the RH. They stated that hydrophobic nature of cyclohexane and chlorobenzene molecules hinder their adsorption onto the water layer as well as their penetration through the water film and contacting the TiO$_2$ surface. In another study [64], it was observed that unlike benzene (a hydrophobic molecule), methanol (a hydrophilic molecule) adsorption efficiency increased with increasing RH up to 35%. This behavior was explained by high water solubility of methanol which allows its molecules to penetrate through layers of water and adsorb on the photocatalyst surface. In contrast, formaldehyde adsorption isotherms at low concentration ([HCHO] ∼120 ppbv) revealed that despite the fact that formaldehyde is a hydrophilic compound, at higher humidity level, P25 reaches its complete saturation faster (i.e. 0% HCHO adsorption): 200, 90 and 50 min for 0, 10, and 65% RH, respectively [70].

2.5. Effect of catalyst support

In PCO, lowering the aggregation of photocatalyst nanoparticles and maximizing their exposure to light irradiance and air stream are sought in order to improve the quantum efficiency and adsorption capacity. This objective can be accomplished by immobilization of photocatalyst on support material. The ideal support material should possess several properties including high surface area, high transparency, porous structure, high adsorptive affinity towards VOCs, and stability under UV irradiation. Several studies have considered AC as a suitable candidate for supporting TiO$_2$ in PCO of gaseous VOCs [71–76]. Due to its high affinity for many indoor air VOCs, AC substantially facilitates the adsorption of VOCs on catalytic bed, lowers the adsorption competition between water vapor and pollutants, and increases the concentration of pollutants around TiO$_2$ nanoparticles [77,78]. It was found that employing AC with P25 in PCO of BTEX (benzene, toluene, ethylbenzene, xylene) and formaldehyde could alleviate the negative impact of short residence time and high RH on the conversion of pollutants [72,73,79]. For example, by an increment in RH from 10 to 60%, benzene conversion on bare P25 and P25 immobilized on AC diminished from 57.5 to 5.6% and 74.3–60.5%, respectively. Similarly, shortening the residence time from 3.7 to 0.6 min caused a conversion drop of ca. 42% for *o*-xylene over P25 against ca. 35% over P25/AC [73]. Lu et al. [72] emphasized on the synergetic relation between AC and TiO$_2$ nanoparticles in PCO process. They demonstrated that photocatalytic destruction of formaldehyde by TiO$_2$ gives rise to an in situ regeneration of AC (via migration of formaldehyde from the internal surface of AC to the external surface (around TiO$_2$ particles)) and delays AC saturation. Thevenet et al. [43] showed that although coupling TiO$_2$ with activated carbon slightly increases the degradation rate of acetylene, it significantly lowers the mineralization to CO$_2$, from 100% to 59.6%, due to the strong adsorption of acetylene on activated carbon. Similarly, Yoneyama and Torimoto [80] claimed that supports with high adsorption constants, such as AC, would retard the diffusion of adsorbed pollutants to the reaction surface (i.e. TiO$_2$) and decrease the decomposition rate. Verbruggen et al. [29] compared the PCO of ethylene over self-supporting Aerolyst 7710 pellets with the same photocatalyst coated on glass beads. The considerable improvement in the removal efficiency of ethylene (up to 70%) for TiO$_2$-coated glass beads was mainly attributed to the longer contact time between ethylene molecules and photons and the increased light scattering inside the reactor [25]. In some cases binder is utilized for the deposition of photocatalyst on the support material in order to improve the stability of photocatalyst. For instance, Thevenet et al. [43] employed silica binder to fix P25 on non-woven organic fibers and showed that the initial degradation rate in the presence of the binder, 1.0×10^{-7} mol L^{-1} min^{-1}, is much lower than the one in the absence of binder, 2.3×10^{-7} mol L^{-1} min^{-1}. Lillo-Rodenas et al. [71] and Bouazza et al. [24] examined the photocatalytic activity of combination of P25 with a number of carbonaceous materials (such as AC, carbon nanotubes, and carbon nanofibers) and white additives (such as zeolites, SiO$_2$, and Al$_2$O$_3$). Despite the fact that most of the support materials had high surface area and adsorption capacity, the highest propene removal efficiency belongs to bare P25. Even though the authors provided no clear justification, the low photocatalytic performance of "P25 + support" could result from the preparation method: TiO$_2$ powder was mechanically mixed with support [24,71]. By analyzing the SEM images of P25 coated on mordenite and SiO$_2$ (both with high surface area ∼300 m^2/g), Mo et al. [81] found that TiO$_2$ only occupy part of small SiO$_2$ particles leading to larger adsorption constant for P25/SiO$_2$ due to strong adsorbability of silica; however, mordenite big particles support more P25 and favor the reaction rate. Table 2 compares the photocatalytic activity of several commercial photocatalysts with and

Table 2
Effect of support material on the removal efficiency of VOCs.

Compound, concentration (ppm)	Photocatalyst/support	Conversion (%)		Ref.
		With support	Bare TiO_2	
BTEX, 0.02	P25/AC	53–60%	18–48%	[77]
BTEX, 0.02 (high RH)	P25/AC	57.9–63.2%	5.6–8.3%	[73]
Ethylene, 75	Aerolyst 7710/glass beads	95%	25%	[29]
Toluene, 2.12	P25/AC	90%	47%	[82]
Formaldehyde, 0.96	P25/netlike AC and P25/granular AC	79% and 66%	25%	[72]
Toluene, 2.5	P25/Mordenite and P25/SiO_2	40% and 38%	30%	[81]

without support material. As can be noticed, employing a support material has an advantageous impact on the removal efficiency of the VOCs.

3. Influence of operating parameters on photocatalytic oxidation processes

3.1. Influence of airflow rate and residence time

Mass transfer of pollutants from the gas phase to the surface of photocatalyst entails several processes and is a function of airflow conditions, type of pollutant, and properties of photocatalyst [2]. Considering a fixed photocatalyst loading, there is general agreement that airflow rate has a dual antagonistic effect on photocatalytic reactions: (i) as the airflow rate increases, the residence time of VOC molecules inside the reactor decreases which leads to a reduction in the adsorption of the pollutant and lower conversion, (ii) higher airflow rate enhances the mass transfer coefficient between the air and photocatalyst surface, resulting in higher PCO reaction rate [51,58]. Taking into consideration the airflow rates normally applied in heating, ventilation and air conditioning (HVAC) systems, it seems reasonable to rule out the contribution of enhanced mass transfer rate and conclude that any increment in the airflow rate (i.e. shorter residence time) deteriorates the VOC removal efficiency. Furthermore, it should be underlined that depending on the adsorption affinity between the reactants and the photocatalyst/support, VOC removal efficiency behaves differently with variations in airflow rate.

Several studies have pointed out that apart from the heterogeneous reactions on photocatalyst surface, gas phase reactions can also contribute to the removal of VOCs [49,52,83], especially when ozone-generating lamps are utilized. Increasing the airflow rate reduces the contact time between the VOC molecules and reactive species such as hydroxyl radicals, ozone, and superoxide anion, and consequently lowers the removal efficiency. In this regard, Jeong et al. [49] reported that in the absence of photocatalyst, conversion of toluene decreased from 100 to 80% by increasing the airflow rate from 1.0 to 4.0 L/min, corresponding to residence times of 33.0 and 8.3 s, respectively. Bouazza et al. [79] found that benzene conversion over P25 and P25/AC undergoes a sharp decline (up to 72% for P25/AC and 96% for P25) with increasing the airflow rate from 7.5 to 60 mL/min, indicating that the negative effect of shorter residence time dominated the advantage of higher mass transfer. Monteiro et al. [58] examined the PCO of PCE over PC500 and observed that by increasing the airflow rate, PCE conversion steadily declines, while oxidation rate firstly increases with flow rate up to Q = 150 cm^3/min (or residence time of 88 s) and decreases afterwards. In another work from the same group [37], it was shown that regardless of the type of photocatalyst (PC500 or P25) and light intensity, conversion of n-decane and PCE diminished at higher airflow rates, whereas VOCs' reaction rates experienced ascending trends. For instance, around 90% of n-decane and PCE were degraded over both PC500 and P25 at 75 cm^3/min, while at 300 cm^3/min, the conversions of n-decane and PCE declined on average by 15 and 25% over PC500

and by 35 and 45% over P25, respectively [37]. As can be noticed, PC500 is less negatively affected by higher airflow rate compared to P25 owing to its higher surface area. In accordance with this reasoning, it was reported that for a long residence time (3.7 min), P25 and P25/AC BTEX-removal efficiency differs marginally, while at a shorter residence time, 0.6 min, and depending on the VOC, P25/AC has removal efficiency of 10–35% higher than P25 [77]. The airflow rate can also influence the amount of by-products formed during PCO reactions. Farhanian et al. [84] investigated the removal efficiency and by-products generation during ethanol photocatalytic oxidation using ozone-generating UV lamps. By increasing the flow rate from 40.3 to 257.1 m^3/h (corresponding to residence times of ca. 80 and 12 ms), ethanol removal efficiency diminished by 50%. Moreover, lower amounts of formaldehyde and acetaldehyde (as ethanol PCO by-products) were obtained at the outlet stream due to shorter residence time of reactants and higher amount of unreacted ethanol. In another study, Vincent et al. [85] found that by increasing the residence time 1-propanol conversion and by-products (propionaldehyde and acetaldehyde) concentrations in the outlet stream significantly increased. Sleiman et al. [86] observed that in spite of the inverse relationship between the airflow rate and toluene conversion, mineralization seems to be independent of the airflow rate suggesting that the applied residence times are sufficient to complete the reactions leading to CO_2. In marked contrast to this study, it was found that the mineralization rate of toluene, isopropyl alcohol, and TCE dropped up to 50% by increasing the airflow rate [87]. Lu et al. [72] showed that at high formaldehyde concentration (~1 ppm), the removal efficiency over P25/AC and bare P25 maximize at a specific airflow rate; however at low concentration (0.3 ppm), the effect of increasing airflow rate was solely negative and the removal efficiency decreased continuously and sharply with face velocity (e.g. over P25/AC: 100% at 0.4 cm/s and 70% at 0.8 cm/s). The works of Lu et al. [72] and Monteiro et al. [58] convey this message that the extent of influence of airflow rate on PCO reaction rate and removal efficiency can considerably vary based on the concentration of pollutant, light intensity, and photocatalyst/support.

3.2. Influence of type and concentration of pollutant

One of the major shortcomings of the previous studies conducted on photocatalytic degradation of VOCs is the evaluation of performance at high VOC concentrations (ppm range) rather those associated with the indoor environment (ppb range). Nevertheless, for various classes of VOCs and broad ranges of concentration, there is general agreement that higher concentration of VOC results in an improved reaction kinetics (until rate reaches its plateau), lower removal efficiency, and poorer mineralization of pollutants to CO_2 [81,87–90]. The impact of higher VOC concentration on PCO reactions can be analyzed from different aspects: (i) the number of VOC molecules that can be adsorbed and oxidized on photocatalyst surface increases which boosts the reaction kinetics [37]; (ii) the ratio of reactive species plus active sites to pollutant molecules decreases and consequently, more VOCs can leave the reactor

without undergoing degradation [90]; (iii) high amount of by-products/intermediates generated during PCO reactions can reduce the mineralization and/or occupy part of the active sites, impeding the oxidation progress.

The effect of pollutant concentration and type on photocatalytic degradation kinetics has been investigated by many researchers [14,15,61,84]. Jafarikojour et al. [51] observed that by increasing the inlet concentration of toluene from 20 to 100 ppm at 30% RH, the conversion decreased from 37% to ca. 27%. Similarly, Mo et al. [81] found that decomposition efficiency of toluene dropped ca. 30% by increasing toluene concentration from 1 to 4 ppm. In another study, Vildozo et al. [56] showed that increasing the inlet concentration of 2-propanol from 100 to 700 ppb significantly lowered the mineralization rate from ca. 90% to 63%. Through their investigations on the PCO of alkanes, Boulamanti and Philippopoulos [61] attained the following order for the apparent oxidation rate: n-pentane < i-pentane < n-hexane < i-hexane < n-heptane. Based on this sequence, they proposed that the presence of a tertiary carbon atom in branched alkanes enhanced the reaction rate. These results are in good agreement with Djeghri et al.'s work [91] which also concluded that generally the reactivity is enhanced as the number of carbon atoms in the chain increases. In the case of aromatic compounds, it was found that the removal efficiency increases in the following order: benzene < toluene < o-xylene < ethylbenzene over bare P25, and benzene < o-xylene < ethylbenzene < toluene over P25/AC; implying that toluene conversion is affected the most by adsorption on activated carbon [73]. Similar sequence was also reported for photocatalytic degradation of aromatic compounds over P25 [63,92]. Boulamanti et al. [63] showed that as concentration increases, almost for all tested aromatics, reaction rate improves until it reaches a plateau. Yu et al. [67] revealed that photocatalytic rate constants of toluene, p-xylene, and m-xylene are directly proportional to their rate constants of reaction with hydroxyl radical ($K_{OH} \times 10^{12}$ (cm^3/molecule s) = 5.96, 14.3, and 23.6 for toluene, p-xylene, and m-xylene, respectively). Interestingly, this positive linear relationship between K_{OH} and PCO reaction rate constant was not found between different classes of organic compounds. Jeong et al. [49] obtained higher removal efficiency for toluene (82.6–99.9%) compared to benzene (67.1–94.2%), and ascribed this behavior to the higher reaction rate of toluene with hydroxyl radicals in the gas phase and on P25. Considering the principles of catalytic reactions, at low pollutant concentration (number of VOC molecules « number of photocatalyst active sites), the reaction rate increases with pollutant concentration until it reaches a region (i.e. intermediate VOC concentration) where the reaction rate becomes independent of concentration [93]. Most of the researchers believe that any further increment in the concentration of pollutant neither improves nor deteriorates the reaction rate since photocatalyst is working at its maximum capacity [86,88,93,94]. On the contrary, investigations on the PCO of benzene [55] and toluene [95] showed that at higher concentration due to the deposition of refractory reaction intermediates on photocatalyst surface and loss of active sites the reaction rate dramatically drops. Similarly, Monteiro et al. [58] observed that under low light intensity, conversion and reaction rate of PCE firstly increases with concentration and then decreases. The noted downward trend for reaction rate was attributed to the lack of photogenerated e−-h+ and surface flooding due to an excessive PCE load.

3.3. Influence of relative humidity

Water molecules can connect to different types of OH surface groups on TiO_2 via hydrogen bond. In addition, water molecules can attach to each other by hydrogen bond and generate well-organized network of adsorbed water layers. The attraction forces between the reactants and TiO_2 are adversely affected by the water layer and in order to be adsorbed on the surface, pollutants must break or disorganize the water network [96]. Before embarking on a discussion of the role of humidity in PCO, it is important to emphasize that in spite of the wealth of literature on the effect of humidity, still no general relationship can be put forward between the VOC removal efficiency, mineralization degree, or reaction rate with the humidity level. Several groups [58,79,85,97–99] recognized a promoting effect of humidity whereas others found the presence of water vapor in PCO inhibiting [25,58,61,86,93,100,101]. On the other hand, some studies have demonstrated that depending on the experimental conditions (e.g. VOC type and concentration, RH range, catalyst loading, and catalyst/support adsorption capacity), a dual effect, positive and negative, of RH can be realized [16,37,52,62,93,102]. In general, water vapor can have two sets of conflicting functions:

I (a) adsorbed water molecule is oxidized to hydroxyl radicals which improves the PCO reactions; (b) RH maintains the oxidation rate by replenishing surface hydroxyl groups [52,55]; and (c) surface hydroxyl groups can trap holes and hinder e−-h+ recombination.

II (a) water molecules adsorbed on the surface of TiO_2 via hydrogen bonding with hydroxyl groups form a multi-layer film which impedes pollutants from contacting TiO_2 surface or reactive species in the boundary layer [94]; (b) water molecules compete with VOCs for adsorption on active sites of TiO_2 [52]; and (c) at very high RH, water vapor can lower the light intensity on photocatalyst surface by blocking the UV radiation.

Taking into consideration the opposing effects of RH, there could be an optimal value of RH before which hydroxyl radical population determines the PCO rate (i.e. efficiency ascends with RH) and after that the inhibiting effect of competitive adsorption dominates the oxidation rate (i.e. efficiency descends with RH). Doucet et al. [103] observed that the maximum conversion of benzene over P25 for long operations can be achieved under 30% RH condition. Using P25 illuminated by an ozone-generating lamp, Kibanova et al. [104] found that the optimum value of toluene removal rate is obtained at RH = 10% and increasing RH to 66% can result in 30% reduction in the reaction rate. The 10% RH was also suggested to maximize the removal efficiency of toluene [52] and formaldehyde [70] over P25. In several studies, it has been demonstrated that the optimal value for RH shifts towards higher values as VOC concentration increases [16,62,68,102]. For instance, it was showed that by increasing the concentration of cyclohexane from 2.2 to 54.5 ppm, the optimal value of RH increased from 22.13 to 26.8% [68]. Mo et al. [16] noticed that in PCO of toluene with concentration between 90 and 250 ppb, increasing the humidity level is solely inhibiting, while at higher concentrations (400–800 ppb), an optimal value for RH exists which maximizes the removal efficiency. Jeong et al. [49] reported that the conversion of toluene ([Toluene] = 10 ppm) improved with increasing RH, reached its peak at RH = 40–50% and then remained constant till RH = 80–90%. This trend was attributed to the fact that large amount of P25 loading resolved the competition effect between toluene and water molecules; therefore, no reduction of conversion was noticed at higher humidity. Einga et al. [97] noticed that higher RH (in the range of 0–60%) had a positive effect on toluene, benzene and cyclohexene decomposition rate, whereas it dramatically decreased cyclohexane PCO rate. Vincent et al. [105] revealed that the RH in the range of 0–30% has no significant influence on photocatalytic conversion of acetone and MEK (504.2 and 406.8 ppm respectively) over P25. The same behavior was reported for benzene, ethylbenzene, and o-, m-, p-xylenes (21–93 ppb) at RH = 18–78% [106], decane (34–810 ppb) at RH = 0–50% [17], and PCE (574–2442 ppm) at RH = 12–40% [90].

Sleiman et al. [86] argued that the reason for negligible impact of RH on PCO of toluene over PC500 is the fact that h+-mediated oxidation was the dominant reaction pathway compared to the oxidation by hydroxyl radicals. Bouazza et al. [79] found that unlike propene for which higher RH negatively affects the conversion, in the case of benzene, presence of RH especially for short residence times is crucial to achieve high conversion. On the contrary, Qijin et al. [64] reported that the conversion of methanol boosted from 55 to 75% by rising the RH from 5 to 20%, while both benzene adsorption and conversion diminished at higher RHs. It is worth mentioning that some studies showed that in the absence of water vapor, photocatalytic degradation of VOC significantly drops [107–109]. In this regard, by comparing the FTIR results of P25 before and after the reaction, it was revealed that the —OH band was completely diminished after PCO of benzene in dry air for 5 h, proving the consumption of hydroxyl groups in the absence of water [110] and suggesting a possible source of efficiency diminution.

Besides the removal efficiency and reaction rate, RH can also play a significant role in the mineralization, intermediates type and by-products amount. In this regard, it was showed that despite the negative/neutral impact of RH on toluene removal efficiency, toluene mineralization to CO_2 was tremendously improved at higher RH [101,111]. Vincent et al. [85] stated that humidity (RH = 0–30%) has a positive effect on 1-propanol (in ppm level) conversion, and simultaneously suppresses the generation of undesirable by-products (e.g. propionaldehyde and acetaldehyde) owing to the larger OH radical population at high RH. In marked contrast, Thevenet et al. [112] found that increasing the humidity level significantly decreases acetylene removal and CO_2 formation rates over P25. They showed that by increasing the relative humidity from 0 to 56%, acetylene removal rate and CO_2 formation rate drastically dropped from 28 to 6 ppm/min and from 48 to 8 ppm/min, respectively. Similar to this study, it was observed that increasing the RH level from 0% to 80% leads to a considerable decrement in mineralization of 2-propanol (in ppb level) from 90% to 20% and toluene (in ppb level) from 95% to 50% [56,86]. These results were further confirmed in PCO of 2-propanol/toluene binary mixtures at ppb levels [66]. Depending on the initial concentration and the ratio between 2-propanol and toluene, increasing the RH from 0 to 60% led to a substantial reduction, ranging from 40 to 70%, in total mineralization [66]. Debono et al. [17] examined the PCO of decane at ppb level and found that water vapor delay the elimination of intermediates and significantly increases their quantities. The observations in these two studies [17,66] can be explained by taking into consideration several outcomes of elevating RH level: (i) adsorption competition between water and reactants; (ii) desorption of weakly adsorbed intermediates (e.g. acetone in PCO of 2-propanol) from the surface to the gas phase; (iii) generation of strongly adsorbed species at higher RH levels which lower CO_2 selectivity and block active sites; and (iv) due the abundance of hydroxyl radicals, high molecular weight (MW) intermediates are more easily decomposed into low MW compounds.

At high humidity levels, owing to the presence of the multi-layer water film, hydrophilicity/hydrophobicity of VOC may exert significant influence on the mass transport of VOC molecules to the surface. Vildozo et al. [66] showed that for the binary mixture of 2-propanol/toluene as the RH increased from 0 to 60%, conversion of 2-propanol reduced only by 5%, while toluene conversion was halved. This was attributed to the fact that unlike toluene, for 2-propanol high affinity toward TiO_2 surface and high water solubility facilitate its penetration through the water film and adsorption on PC500 surface [66]. Zhang et al. [69] suggested that due to the hydrophobic nature of chlorobenzene, it can be speculated that molecules can adsorb on the water film and react with active species in the water phase. In the case of ethylene, which is nonpolar, it was observed that an initial region of rapid decrease
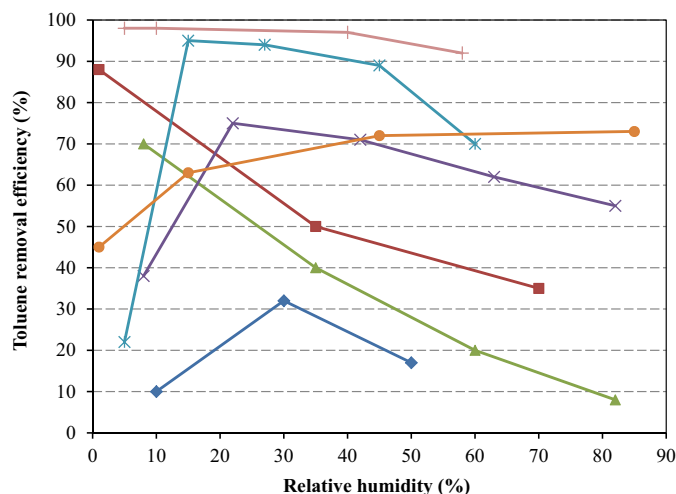

Fig. 2. Influence of relative humidity on toluene photocatalytic removal over P25: (♦) [51], (■) [101], (▲) [77], (×) [62], (*) [16], (+), low concentration) [16], (●) [49].

(65% decline in reaction rate by increasing RH from 0 to 40%) is followed by a slower, steady decrease in the oxidation rate as RH increases [94]. Interestingly, Kibanova et al. [70] demonstrated that the competition of water molecules for active sites and saturation of smaller pores of photocatalyst reduced the efficiency of photocatalytic oxidation of both hydrophobic (toluene) and hydrophilic (formaldehyde) pollutants [70]. Yu et al. [98] found that increasing the RH level (30–70%) improves the PCO of toluene to a greater extent than that of formaldehyde, possibly due to the difference in hydrophilicity of formaldehyde and toluene. Fig. 2 attempts to demonstrate that even though these studies use the same photocatalyst and pollutant, the impact of RH on toluene removal efficiency does not follow a unique trend and varies based on specific operating conditions employed in each research.
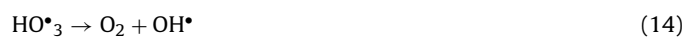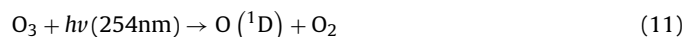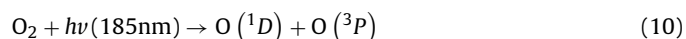
3.4. Influence of light source and intensity

As discussed in section 1, light is one of the main pillars of photocatalysis; therefore, light source wavelength (WL) and light intensity (I) can affect the reaction rate and removal efficiency. Considering the band gap energy of commercial photocatalysts listed in Table 1, theoretically, UV light with wavelength less than 380 nm can excite the electrons in the valence band [21,55]. Germicidal lamp (UVC, 254 nm) and fluorescent black-light lamp (300–400 nm) are the most utilized light sources in PCO of indoor air pollutants. Some studies employed UV light emitting diode (wavelength usually centered at 365 nm) due to long lifetime and high efficiency [30,113]. For the same photon energy distribution, i.e. light wavelength, increasing the light intensity leads to generation of a larger number of photons and consequently e−-h+ pairs. It is proposed that the impact of UV intensity on the reaction rate can be divided into two regimes: (i) a first-order regime at low light intensity and high VOC concentration where e−-h+ pairs are consumed faster by chemical reactions than by recombination and (ii) a half-order regime at high light intensity and low VOC concentration in which the rate of recombination exceeds the rate of oxidation reactions [114].

The aforementioned relationship between light intensity and reaction rate has been reported for TCE [115] and 1-propanol [85] with the transition from first to half-order regime at about 1.5 and 4 W/m2, respectively. It should be mentioned that even though increment in light intensity brings about higher pollutant removal efficiency, excessive light intensity diminishes quantum efficiency and imposes unnecessary energy cost [93]. In this regard, Tang and

Yang [95] suggested a novel method to determine the maximum required light intensity based on the VOC molecule type, average reaction rate, optical absorption coefficient of photocatalyst, and light wavelength. Einaga et al. [55] examined the rate of benzene photooxidation by P25 ([Benzene] = 125 ppm; RH = 50%; residence time = 20–40 s) and found that by doubling the light intensity, reaction rate improves roughly by 50%. In a similar investigation on PCO of acetone ([Acetone] = 504.2 ppm; RH = 10%; residence time = 12.6 s), Vincent et al. [105] observed that acetone conversion was enhanced from 21% to 63% as the light intensity increased from 2.1 to 39.4 W/m². A comparison between photocatalytic conversions of 17 VOCs at high concentrations (400–620 ppm) using black light or germicidal lamp with the same power output revealed that there is no substantial performance difference between the two light sources [65].

In order to improve the removal efficiency and mineralization, many studies [70,104,116] employed ozone-generating UV lights (254 + 185 nm), which may offer a combination of photolysis, ozonation, and PCO processes. Nonetheless, it is noteworthy that using ozone-generating lights can result in high concentrations of ozone at the outlet stream, which necessitates installation of ozone scrubber after PCO section. On the other hand, even though direct ozonation of VOCs in the gas phase has been reported in the literature [117], considering the slow rate of ozonation reactions and short residence time of VOCs in the reactor («1 s), some researchers believe that ozonation may not have significant contribution [70,104,116]. Instead, VOCs can react more rapidly with short-lived reactive species and radicals such as $O(^3P)$, $O(^1D)$, and $OH^\bullet$, produced during the formation and destruction of ozone in the reactor [83,116,118]:

$$H_2O + h\nu(185nm) \rightarrow H + OH^\bullet \tag{9}$$

$$O_2 + h\nu(185nm) \rightarrow O\left(^1D\right) + O\left(^3P\right) \tag{10}$$

$$O_3 + h\nu(254nm) \rightarrow O\left(^1D\right) + O_2 \tag{11}$$

$$O_3 + e^- \rightarrow O^\bullet_3^- \tag{12}$$

$$O^\bullet_3^- + H^+ \rightarrow HO^\bullet_3 \tag{13}$$

$$HO^\bullet_3 \rightarrow O_2 + OH^\bullet \tag{14}$$

$$O\left(^1D\right) + O_2 \rightarrow O\left(^3P\right) + O_2 \tag{15}$$

$$O\left(^3P\right) + 2O_2 \rightarrow O_3 + O_2 \tag{16}$$

$$O\left(^1D\right) + H_2O \rightarrow 2OH^\bullet \tag{17}$$

Kibanova et al. [104] reported that the reaction rate of toluene over P25 under ozone-generating lamp is almost twice of that under UVA illumination. Investigations on PCO of formaldehyde, benzene, and toluene at low concentrations over P25 (<600 ppb) revealed that the removal rate follows the order of $UVC/O_3 > UVC > UVA$ [49,70], likely due to the low-energy photons in the case of UVA and positive involvement of ozone in the PCO reactions for ozone-generating lamp. In a study by Quici et al. [52], reaction rate of toluene in the absence of P25 under 254 + 185 nm UV irradiation was around a quarter of that in the presence of photocatalyst which can be attributed to the gas phase reactions with active oxygen species, direct photolysis, and oxidation by $OH^\bullet$ formed by photolysis of water molecules (Eqs. (9)–(17)). Regarding the effect of ozone on mineralization degree, Krichevskaya et al. [119] observed that by raising ozone concentration in the reactor from 40 to 80 $\mu g\,O_3\,L^{-1}$, CO_2 concentration increased from 7 to about 20 ppm during PCO of a mixture of styrene, acrylonitrile and toluene.

In general, it is widely accepted that increasing light intensity at photocatalyst surface or using light source with a shorter wavelength enhances the removal efficiency and reaction rate

[49,93,105,120]. However, depending on the light intensity, residence time, and VOC type/concentration, production of intermediates/byproducts can be decreased [49,120] or increased [85] with light intensity. Besides the advantageous impact of ozone on PCO reactions, ozone plays a crucial role in hindering photocatalyst deactivation by destruction of carbon deposits on the surface [49,116] and prolonging the $e^- \text{-} h^+$ pair lifetime by capturing the generated electrons [118].

Table 3 presents a summary of photocatalyst/support type, photoreactor, key operating parameters, and the main shortcomings of each study conducted on the photocatalytic degradation of various VOCs over different commercial photocatalysts. Furthermore, Fig. 3 summarizes the removal efficiency of some of the VOCs over P25, PC series and UV100. It can be clearly noticed that none of the photocatalysts possesses superior performance in all cases.

4. Reaction pathways and main intermediates/by-products

Ideally, products of PCO of hydrocarbon VOCs are carbon dioxide and water. However, given the short residence time of reactants and adsorption competition, in reality, VOC mineralization can proceed up to a certain degree and many oxidation by-products/intermediates exist both in the gas phase and on photocatalyst. In fact, generation of by-products is one of the main concerns associated with the application of PCO technology in buildings since some of these by-products can be even more toxic than their parent compounds. Based on the type of challenge compound, different reaction pathways have been proposed and various by-products/intermediates have been identified in photocatalytic degradation of VOCs.

4.1. Alcohols

Muggli et al. [131] employed isotope labeling and temperature-programmed desorption and oxidation (TPD-TPO) to identify the reaction pathways and intermediates for PCO of ethanol over P25. Based on the obtained results they suggested two reaction pathways: (a) ethanol → acetaldehyde (widely accepted as the first step in PCO of ethanol) → acetic acid → CO_2 + formaldehyde → formic acid → CO_2 and (b) ethanol → acetaldehyde → formic acid + formaldehyde → formic acid → CO_2. A similar mechanism was put forward by Nimlos et al. [60]: ethanol → acetaldehyde → acetic acid → formaldehyde → formic acid + CO_2 → CO_2. A proposed reaction pathway for PCO of ethanol is depicted in Fig. 4 [132].

Benoit-Marquieí et al. [133] proposed the following degradation mechanism during 1-butanol photocatalytic degradation: 1-butanol → butanal → butanoic acid → propionaldehyde and 1-propanol. In agreement with this study, it was found that butanal and 1-butene are the two major by-products of PCO of 1-butanol over P25 at low [134] and very high concentration [135]. Kirchnerova et al. [31] reported that the initial rates of formation of three main intermediates (butanal, propionaldehyde, acetaldehyde) as well as n-butanol conversion are faster over P25 compared to UV100. This behavior could stem from higher crystallinity, i.e. lower recombination rate, of P25 since upon UV100 calcination at 623 K, initial n-butanol conversion and butanal and crotonaldehyde production were accelerated. Vincent et al. [85] have considered the attack of $OH^\bullet$ radicals and oxygen mechanism along with several mechanisms of homogeneous gas-phase reactions to explain the reaction mechanisms of 1-propanol. Considering the examples discussed above, it can be inferred that a general reaction pathway for PCO of alcohols could be: alcohols → aldehydes → acids → shorter carbon-chain aldehydes + alcohols → CO_2 and H_2O.

Table 3

Overview of VOCs photocatalytic degradation over various commercial titanium dioxides.

Photocatalyst	Characterization method	Coating method/Catalyst loading (mg/cm^2)	Reactor type and volume (L)	Pollutant	Conc. (ppmv)	RH (%)	Residence time	Light primary wavelength and intensity (W/m^2)	Major limitations				Ref.
									Pollutant Conc.	Res. time	By-product	Other	
P25	SEM	Dip-coated on glass plate; 0.49	Glass-plate photoreactor	Toluene	0–4	47	–	254 nm; 16.4	√	NR	NR	–	[81]
	–	Dip-coated on glass plate; 1.16	Glass-plate photoreactor		0.09–0.8	3–70	0.2 s	254 nm; 43	√	√	√	–	[16]
	–	Dip-coated on Raschig rings	Tubular-flow reactor		0.01–0.5	0–66	0.1–2 s	254 nm; 30	√	√	√	–	[52]
	–	Dip-coated on pyrex glass; 0.15	Cylindrical reactor with coated Raschig rings; 0.55		0.6–10	40	16–47 s	365, 254 and 254 + 185 nm; -	√	×	√	High ozone conc.	[83]
	–	–	Stainless steel plate-type photoreactor		0.450–8	47–50	0.2 s	254 nm; 4.3–9.5	√	√	√	–	[21]
	–	–	Batch Pyrex reactor; 120		0.05–0.8	0–50	–	365 nm; 100	√	NR	√	Batch; High I	[111]
	FTIR, XPS	–	–		40	1–70	–	365 nm; -	×	NR	NR	–	[101]
	XRD, SEM	Immobilized on stainless steel; 0.0274–0.0924	Photoreactor consisted of two coaxial cylinders		20–100	10–50	–	254 nm; 37	×	NR	NR	–	[51]
	–	Dip-coated on Raschig rings	Cylindrical flow reactor with coated Raschig rings		0.17	10–66	0.9 s	365 and 254 + 185 nm; 7.7–28	√	√	√	–	[104]
	–	Immobilized on activated carbon or glass fiber filter	–		2.12	–	–	254 and 365 nm; 14.9–27.6	×	NR	NR	–	[82]
	BET, SEM	Wash-coated on activated carbon	–		–	15–60	–	254 nm; -	×	×	√	–	[99]
	UV–vis	Wash-coated on glass; 2	–	Benzene	80–260	0–65	25 s	365 nm; -	×	×	NR	–	[55]
	FTIR	Coated on optical fiber; 0.85	Batch		20	5	–	365 nm; 10–40	×	NR	√	Low RH	[93]
	FTIR	–	Fixed-bed flow reactor		80–257	zero	–	–	×	NR	√	No RH	[110]
	–	Coated on glass fiber filter; 4	Continuous flow reactor; 18.6	Formaldehyde	0.05–10	10–65	1.2–3.8 min	365 nm; 7.5	√	×	√	–	[107]

Table 3 (*Continued*)

Photocatalyst	Characterization method	Coating method/Catalyst loading (mg/cm²)	Reactor type and volume (L)	Pollutant	Conc. (ppmv)	RH (%)	Residence time	Light primary wavelength and intensity (W/m²)	Major limitations				Ref.
									Pollutant Conc.	Res. time	By-product	Other	
–	–	–	Cylindrical reactor with coated Raschig rings		0.1–0.5	0–66	0.05–0.500 s	365, 254 and 254 + 185 nm; 7.7–44.5	√	√	NR	–	[70]
	–	Coated on AC by Dipping method	Honeycomb		0.3–0.96	30	–	365 nm; 11.8	√	√	NR	–	[72]
	–	Coated on fibreglass support, 2	Annular photoreactor	Acetone	504.2	10	12.6–25.2 s	365 nm; 0–40	×	×	√	–	[105]
	SEM	Coated on quartz fibers by dripping TiO₂ suspension	Optical fiber reactor		50–750	–	2–16 min	–	×	×	√	–	[59]
	XRD, BET, ESR	–	–		400	–	–	365 nm, 5.4	×	×	NR	–	[50]
	SEM	–	Annular reactor packed with catalyst pellets	Ethanol	50	75	–	365 and 254 nm; 34.9–71.7	×	NR	√	–	[120]
		–	Cylindrical photoreactor		62.5	–	–	365 nm; 1.435	×	NR	√	–	[100]
	XRD, BET, TEM, UV–vis	Coated on zeolites, MOF, SiO₂, Al₂O₃, glass wool	Fixed bed reactor	Propene	100	zero	–	257.7 and 365 nm; -	×	NR	NR	No RH	[24]
	BET, TEM, XRD	–	–		100	zero	–	257.7 and 365 nm; -	×	NR	NR	No RH	[71]
	SEM	–	Annular fluidized bed photoreactor	Cyclohexane	2.2–54.5	5–40	–	254 nm; -	×	NR	√	–	[68]
	–	Coated on glass fiber; 2	–	Acetylene	100	zero	2 s	365 nm; 80–100	×	×	√	No RH	[121]
	–	–	Tubular photoreactor; 0.275	PCE	574–2442	12–40	–	253.7 nm; 0.5	×	NR	√	–	[90]
	UV–vis, XRD, BET, FTIR	Dip-coated on glass slide; 2	Glass-plate photoreactor	1-butene	1–9	0	–	352 nm; 6.3	×	NR	NR	No RH	[88]
	–	Wash-coated on glass slide; 0.74	Glass-plate photoreactor	Ethylene	1–1000	0–84	–	352 nm; 56	×	NR	NR	–	[94]
	–	Coated on fibreglass support	Annular photoreactor; 0.0664	1-propanol	100–300	0–30	11.8–25.2 s	365 nm; 0.78–39.4	×	×	√	–	[85]
	–	–	Batch Pyrex reactor; 120	Decane	0.03–0.81	0–50	–	365 nm; 100	√	NR	√	Batch; High I	[17]
	N₂ ads-des, BET, SEM	Coated on activated carbon by spray desiccation	–	Methanol	23.7–34.3	0–80	–	365 nm; -	×	×	NR	–	[122]

Table 3 (*Continued*)

Photocatalyst	Characterization method	Coating method/Catalyst loading (mg/cm²)	Reactor type and volume (L)	Pollutant	Conc. (ppmv)	RH (%)	Residence time	Light primary wavelength and intensity (W/m²)	Major limitations				Ref.
									Pollutant Conc.	Res. time	By-product	Other	
–	–	–	–	Formaldehyde, Toluene, 1, 3-butadiene	0.07–100	0–93	–	90–400	√	√	NR	High I	[62]
	–	Dip-coating on glass/stainless steel	Annular photoreactor	Benzene, ethyl-benzene, xylene	0.004–0.034	10–100	5 s	352 nm; 38	√	×	√	–	[123]
	–	Dip-coating on glass tube; 3.2	Plug flow photoreactor; 0.405	TCE, octane, acetone, methanol, MEK, propanol, BTE, xylenes	400–600	23	2.025 min	365 and 254 nm; -	×	×	√	High T	[65]
	–	3.5	Annular photoreactor; 0.02	BTE, xylenes	0–34	0	50–210 s	254.7 + 184.9 nm; -	√	×	√	No RH	[63]
	–	Coated on glass fiber filter or activated carbon	–	BTE, xylenes	0.02	10–82	0.6–3.7 min	365 nm; 7.5	√	×	NR	–	[73]
	–	Dip-coated on pyrex glass; 0.15	Cylindrical flow reactor with coated Raschig rings; 0.55	Toluene, benzene	0.6–10	0–90	8.3–33 s	365, 254 and 254 + 185 nm; -	√	×	√	–	[49]
	–	Coated on pyrex tube; 0.5	Tubular-flow reactor	Benzene, ethyl benzene, xylenes	0.021–0.093	18–78	0.7–5.1 s	352 nm; 22–58	√	×	√	–	[106]
	–	Wash-coated on alumina ceramic foam; 0.74	Glass-plate photoreactor	Formaldehyde, toluene	0.17–20	0–93	–	352 nm; 3.3–7.1	√	NR	NR	–	[102]
	BET, SEM	Coated on glass fiber filter or AC filter; 4.1	–	BTE, xylenes	0.02	7.5–82	0.6–3.7 min	365 nm; 7.5	√	×	NR	–	[77]
	–	3.6	Honeycomb	Toluene, formaldehyde	2	30–70	–	254 nm; 0.49	×	NR	NR	–	[98]
		Coated on cellulose fibers or aluminum honeycomb; 0.4	–	Methanol, toluene	100	–	–	254 nm; -	×	NR	NR	–	[124]
	XRD, SEM, AFM	Coated on glass spherules	Photocatalytic packed bed reactor	Benzene, toluene, xylenes	10.5–350.5	60	–	350 nm; -	×	NR	NR	–	[125]
	–	3.5	Annular photoreactor; 0.02	Pentane, *i*-pentane, hexane, *i*-hexane, heptane	0–100	0–90	50–85 s	254.7 + 184.9 nm; -	√	×	√	High T	[61]
	–	Dip-coated on glass; 1.55	Glass-plate photoreactor	Toluene, *o*-xylene, benzene	0–3.5	45	–	254 nm; 2.34	√	NR	√	–	[95]

Table 3 (*Continued*)

Photocatalyst	Characterization method	Coating method/Catalyst loading (mg/cm²)	Reactor type and volume (L)	Pollutant	Conc. (ppmv)	RH (%)	Residence time	Light primary wavelength and intensity (W/m²)	Pollutant Conc.	Res. time	By-product	Other	Ref.
									Major limitations				
	UV–vis, FTIR	–	Flow-type photoreactor	Benzene, toluene, cyclohexene, cyclohexane	493–514	0–70	–	–	×	NR	NR	–	[97]
	–	Wash-coated on glass plate; 1.05	Glass-plate photoreactor	Toluene-Benzene	0.57–7.3	40	–	5.6	√	NR	NR	–	[126]
	N_2 ads-des	–	–	Propene, benzene	100	0–93	–	257.7 nm; 57	×	NR	√	–	[79]
PC500	–	–	–	Toluene	–	0–95	–	–	NR	NR	√	–	[89]
	–	Coated on non-woven fibrous paper; 0.5	Stainless steel annular flow-through; 0.085		0.02–0.4	0–70	0.8–4 min	43	√	×	√	–	[86]
	–	Coated on non-woven paper; 0.5–2	Stainless steel annular flow-through; 0.05	2-propanol	0.100–0.7	0–60	6–30 s	32	√	×	√	–	[56]
	–	Coated on non-woven fibrous papers; 1.8	continuous flow-through reactor; 0.085		0.05–0.7	0–80	17–102 s	43	√	×	√	–	[127]
	–	non-woven paper; 2	Stainless steel tubular flow-through photoreactor; 0.05	2-propanol, Toluene	0.08–0.4	0–60	10 s	32	√	×	√	–	[66]
	–	Dip-coated on cellulose acetate monolithic	Annular photoreactor; 0.22	PCE	600–2200	3–40	>44 s	280–400 nm; 18.9–38.4	×	×	√	–	[58]
Aerolyst 7710	–	–	Batch photoreactor	Acetaldehyde	5000	–	–	310–400 nm; 81	×	×	√	Batch	[128]
	BET	Washed coated on glass beads washed	Packed bed tubular reactor	Ethylene	75	–	1.02 s	254 nm; 0.87	×	×	√	–	[29]
	BET, N_2 ads-des, XRD	Coated on glass beads	Fixed bed photocatalytic		50–100	0–25	–	254 nm; -	×	NR	NR	High T	[25]
UV100	SEM, BET, XRD, XPS	Embedded in carbon nanofiber	stainless steel reactor; 0.02	Acetaldehyde	15	–	–	–	×	NR	NR	–	[129]
P25, PC500	XRD; N_2 ads-des, UV–vis	Coated on glas slides;	Batch photoreactor	Toluene, Formaldehyde	3–49	–	–	36.4	×	×	√	Batch	[27]

Table 3 (*Continued*)

Photocatalyst	Characterization method	Coating method/Catalyst loading (mg/cm^2)	Reactor type and volume (L)	Pollutant	Conc. (ppmv)	RH (%)	Residence time	Light primary wavelength and intensity (W/m^2)	Major limitations				Ref.
									Pollutant Conc.	Res. time	By-product	Other	
	BET, XRD, UV–vis	Immobilized on glass beads by suspension	Continuous gas flow reactor	Acetaldehyde	100–170	zero	–	365 nm; 2	×	NR	√	No RH	[47]
	–	Coated on cellulose acetate monolithic	Annular photoreactor; 0.22	*n*-decane, PCE	75–2738	3–40	44–130 s	18.9–38.4	×	×	NR	–	[37]
	SEM	Dip-coated on inorganic/organic fibers	Batch Pyrex reactor; 0.35	Acetylene	1100	0	–	43	×	NR	√	No RH	[43]
PC500, PC50, P25	UV–vis, XRD, BET, TGA	–	Fluidized bed reactor; 0.02	MEK	250–1000	3.7	–	365 nm; 900	×	NR	NR	High I and T; Low RH	[30]
PC500, PC105, P25	–	Coated on cellulose fibers, aluminum and quartz plates	–	n-octane, Methanol	37–356	0	–	100	×	NR	√	No RH; High I	[32]
P25, PC100, UV100	FTIR, BET, XRD	–	Packed-bed cylindrical photoreactor	2-propanol	–	100	~1 min	–	NR	×	√	–	[46]
PC105, P25	XPS, FTIR, BET, XRD, SEM, TEM, UV–vis	–	Batch P glass cylindrical reactor; 5	Acetone, acetaldehyde, toluene	400	–	–	315–400 nm; 30	×	×	NR	Batch	[28]
UV100, P25	–	–	Cylindrical reactor with tubular lamp; 1.72	n-butanol	145–580	1.7	–	–	×	NR	√	Low RH	[31]
	SEM	Supported on a fibreglass mesh	Batch	Acetone	840.4	zero	–	–	×	NR	NR	Batch; No RH	[130]
	XRD, BET, TGA, TPO, XPS	Coated on Pyrex tube; 0.11–2.23	Annular Pyrex reactor made of coaxial tubes	MEK	1500	50	7.6–19 s	380 nm; 33	×	×	√	–	[26]

NR = not reported; Conc.: Concentration; Res.: Residence.
BTE: benzene, toluene, ethylbenzene; T: Temperature; I: Light intensity; RH: Relative humidity.
In all works, experiments were conducted at room temperature unless otherwise is stated.
XPS: X-ray photoelectron spectroscopy; ESR: electron spin resonance; N$_2$ ads-des: nitrogen adsorption desorption test; AFM: atomic force microscope.
√ = for concentration means experiments in ppb level were included in the study; for residence time means experiments with short residence time (1 s) which are close to the real application were included in the study; for by-product identification means quantification/qualification of by-products/intermediates were included in the study.
× = for concentration means all experiments were conducted at pollutant concentration greater than 1 ppm; for residence time means all experiments were conducted at high residence time (>1 s).
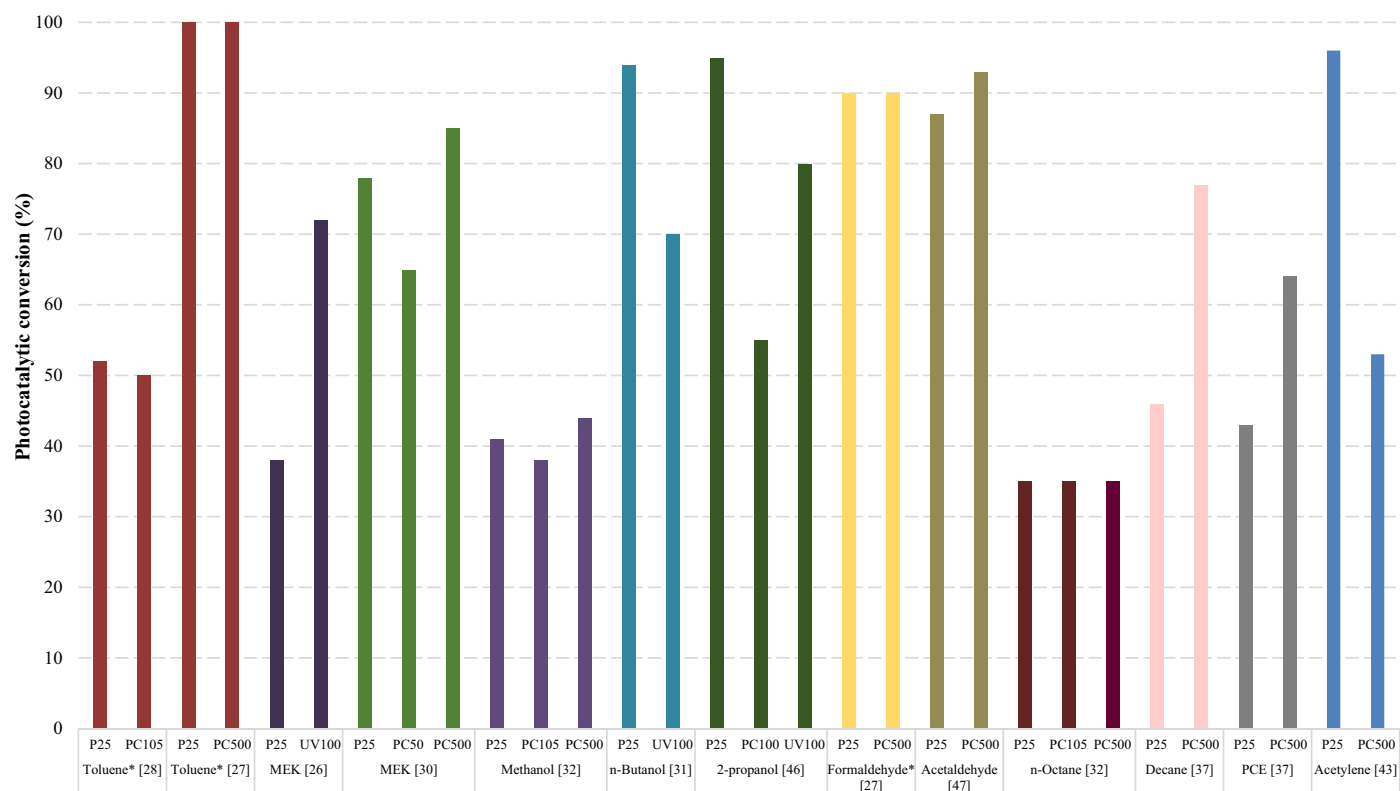
Fig. 3. Comparison between photocatalytic performances of different photocatalysts in degradation of VOCs; *experiments were conducted in batch reactor.
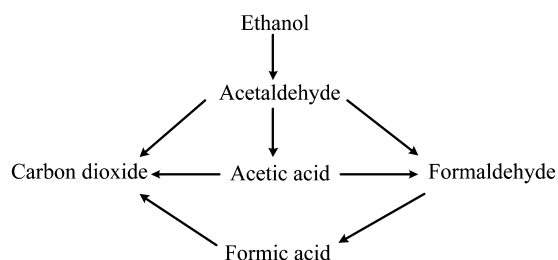

Fig. 4. Reaction pathway for photocatalytic oxidation of ethanol [132].

4.2. Aromatics

Photocatalytic oxidation of toluene and benzene have been examined extensively and, accordingly, many studies have been focused on the identification/quantification of reaction intermediates. It is suggested by many researchers that PCO of benzene and toluene entails the generation of strongly adsorbed intermediates (often accompanied by change of photocatalyst color from white to yellow) which are less reactive than their parent compounds [21,48]. In the case of toluene, benzaldehyde, benzoic acid, benzyl alcohol, phenol and benzene have been found to be the first reaction intermediates [21,28,48,136]. d'Hennezel et al. [48] proposed a step-by-step reaction pathway for PCO of toluene over H_2O/HCL pretreated P25. It was suggested that the primary pathway is hydrogen abstraction from methyl group and benzyl radical formation via hole transfer to toluene, hydrogen abstraction by an OH radical, and hydrogen abstraction by chlorine radical [48].

Toluene can be adsorbed on TiO_2 surface through the formation of an OH...π electron type complex on hydroxylated surface and via the formation of a Ti^{4+}...π electron type complex on dehydroxylated surface. Given this fact, Sleiman et al. [86] stated that

the humidity content influences the adsorption mode of toluene on PC500 and, therefore, brings about two competitive initial reaction pathways: (i) at low RH, h^+-mediated reactions lead to the formation of an aromatic radical cation and a benzyl radical, followed by further oxidation and aromatic ring opening reactions; (ii) at high RH, the first step is the addition of OH radical on the aromatic ring or the H-abstraction from the methyl group. Fig. 5 demonstrates the proposed reaction pathways by Sleiman et al. [86] for toluene PCO. Furthermore, they reported that benzaldehyde and benzene were the main gaseous intermediates under both dry and humid conditions, while methyl vinyl ketone (MVK) and methyl glyoxal were measured only at dry condition, and cresols, benzyl alcohol, and phenol were detected only at 40% RH.

Based on the detected by-products in gas phase and on P25 surface using proton transfer reaction-mass spectrometer (PTR-MS) and gas chromatography–mass spectrometry (GC/MS), Mo et al. [21] put forward a complicated and comprehensive reaction pathway for toluene PCO. They considered OH radical induced aromatic ring opening mechanism, previously suggested by Frankcombe and Smith [137], for toluene and its three initial by-products (benzaldehyde, benzoic acid, and benzyl alcohol) and proposed the following reaction mechanism: toluene → benzaldehyde → benzoic acids → ring broken → O=C—R—C=C—R'—C=O → shorter-carbon-chain aldehydes and alcohols. Using TPD-TPO, Larson and Falcon [136] identified benzaldehyde, benzyl alcohol and m-cresol as intermediates of photodegradation of toluene on P25. In toluene PCO, formaldehyde generation strongly depends on RH, suggesting that the abundance of OH groups on P25 surface could be the reason for formation of formaldehyde [52]. Mo et al. [16] observed that there is no linear relationship between humidity and the amount of produced intermediates for most of the intermediates in toluene PCO; nonetheless, depending on the inlet concentration of toluene, RH in
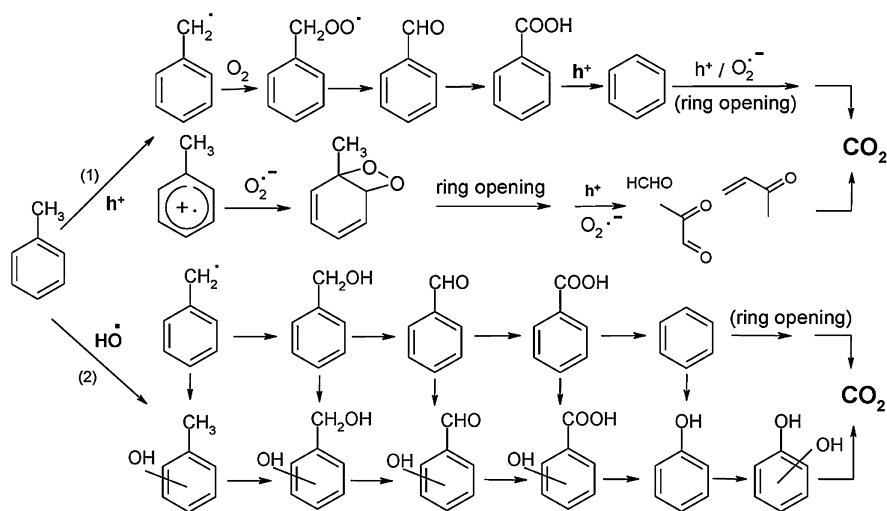
Fig. 5. Reaction pathway for photocatalytic oxidation of toluene as proposed by Sleiman et al. [86].

the range of 10–20% resulted in the lowest amount of by-products in the gas phase.

4.3. Aldehydes

Ao et al. [107] proposed a reaction pathway for formaldehyde photocatalytic degradation over P25 which starts with the generation of formic acid via direct photolysis and photocatalysis, followed by h^+-mediated conversion of formic acid into carbon dioxide. Ye et al. [138] examined PCO of butanal and proposed a reaction pathway as follows: aldehydes → acids → shorter carbon-chain aldehydes. In another study, Hauchecorne et al. [128] proposed a relatively complicated reaction pathway for PCO of acetaldehyde over TiO_2 using FTIR in situ reactor. Acetaldehyde is adsorbed on TiO_2 surface where it undergoes aldol condensation (formation of 3-hydroxybutanal and crotonaldehyde) and oxidation reactions (formation of bidentate acetate bound on the surface). These initially formed species are converted into other intermediates such as acetic acid, formic acid and formaldehyde upon further illumination. Fig. 6 displays the mechanistic scheme of PCO of acetaldehyde proposed by Hauchecorne et al. [128].

Verbruggen et al. [47] stated that the reaction pathway for PCO of acetaldehyde may differ over PC500 with regard to that over P25 owing to the smaller population of e^--h^+ pairs on PC500 (discussed in section 2.1). They explained that in the presence of adequate number of holes (i.e. on P25), acetaldehyde is oxidized readily into CO_2, whereas at lower hole concentration (i.e. on PC500) acetic acid is found as an intermediate.

4.4. Alkanes, alkene and alkynes

It has been suggested that the photocatalytic degradation of alkanes entails less complexity in comparison to that of alcohols and aromatic hydrocarbons; therefore, the amount of generated intermediates/by-products is smaller for alkanes [67]. Degradation of alkane is initiated by the abstraction of proton to form alkyl radical which then reacts with oxygen and produces alkyl proxy radical. This alkyl proxy radical can go through reactions with alkane itself or with $HO^\bullet_2$ and generate carboxylic acid [67]. In a research primarily focused on the reaction mechanisms and intermediates of decane PCO over P25, Debono et al. [17] utilized a batch reactor in order to monitor the formation and consumption of reactants and intermediates at each step of the reaction advancement. They reported that during the photocatalytic degradation of 800 ppb

decane under 50% RH, 18 reaction intermediates were identified in the gas phase, mainly from aldehyde, ketone and alcohol families (most abundant: formaldehyde, acetaldehyde, propanal, and ethanol). The general scheme of reaction pathway for decane is shown in Fig. 7 (for in detail explanation regarding each step refer to [17]).

In another study, Einaga et al. [97] suggested that the addition of OH radicals to unsaturated C=C bonds of cyclohexene and also the abstraction of H atoms from saturated C—H bonds of cyclohexane and cyclohexene result in a number of intermediate radicals which are subsequently oxidized by molecular O_2 and eventually converted into CO_2. Thevenet et al. [121] explored the PCO of acetylene over P25 in a continuous flow reactor and focused on the identification of adsorbed species on the surface. They revealed that as the reaction proceeds, high surface coverage by the adsorbed carboxylic acids brings about a considerable release of light compounds such as formic acid, formaldehyde and glyoxal to the gas phase.

4.5. Ketones

Acetone and MEK are the most studied members of ketone family [59,105,139,140]. Vincent et al. [105] put forward three main reaction schemes for PCO of acetone over P25 (two of them chain reactions initiated by OH and aldol condensation as the third one) based on the identified reaction intermediates and their relative abundance which can be ranked in this order: diacetone alcohol > acetic acid > MEK > methyl alcohol > other by-products. Choi et al. [59] stated that at high concentrations, both hydroxyl radical attack and h^+-mediated oxidation pathways are important in PCO of acetone. The reaction schemes suggested by Bianchi et al. [28] for acetone and Raillard et al. [139] for MEK are presented in Fig. 8.

Table 4 summarizes main intermediates detected during photocatalytic degradation of VOCs and also lists some of the prevalent analytical methods employed for intermediates identification/quantification.

5. Photocatalyst deactivation and regeneration

Photocatalyst deactivation leads to a considerable decline in the removal efficiency as well as an increment in the amount of by-products due to partial oxidation of VOCs. In addition, from economic perspective, catalyst's short lifetime can impose frequent
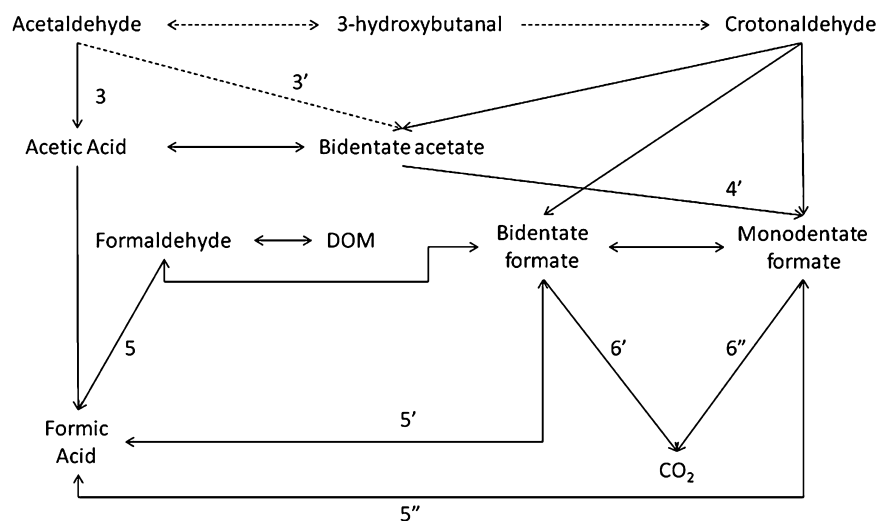
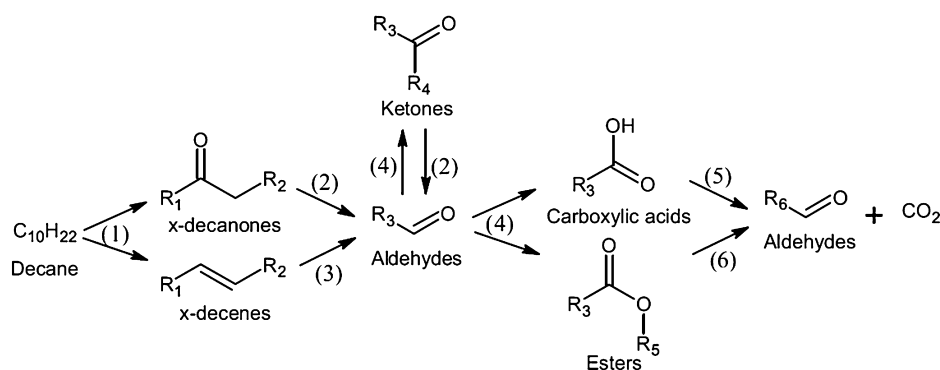**Fig. 6.** Acetaldehyde PCO mechanism as proposed by Hauchecorne et al. [128].

Fig. 7. PCO mechanism of decane proposed by Debono et al. [17].

Table 4
Overview of intermediates for VOCs PCO and analytical techniques for intermediate identification.

Target VOC	Intermediates/By-products	Analytical technique	Ref.
Toluene	Acetone, acetaldehyde, formaldehyde, benzaldehyde, o-cresol	GC/MS, HPLC	[111]
	Benzene, benzyl alcohol, benzoic acid	FTIR	[141]
	Formaldehyde, acetaldehyde and methanol, propylene, acetone, acetic acid, benzene	PTR-MS	[16]
	Acetone, acetic acid, butyraldehyde, benzene, pentanal, benzaldehyde, benzoic acid	PTR-MS, GC/MS	[21]
	Benzoic acid, benzyl alcohol, and benzaldehyde, formic acid, acetic acid	GC/MS, HPLC	[48]
	Benzaldehyde, benzene, formaldehyde, MVK, cresol, phenol, benzyl alcohol	GC/MS, HPLC	[86]
	Benzyl alcohol, benzaldehyde, benzoic acid	GC	[95]
	Benzyl alcohol, benzoic acid, benzaldehyde, hydroquinone, cresol	FTIR	[28]
	Benzyl alcohol, benzoic acid, benzaldehyde, hydroquinone	GC, HPLC	[144]
Benzene	Hydroquinone,4-benzoquinone, phenol, formic, acetic acids	GC/MS, HPLC	[48]
	1,5-hexadien-3-yne, 2,4-hexadiyne, 1,3-hexadien-5-yne, formic acid	GC/MS, FTIR	[93]
	2-propenoic acid, 2-methyl-1-propanol	GC	[95]
Acetone	Acetaldehyde, methyl and isopropyl alcohol, MEK, ethyl acetate, acetic acid, mesityl oxide, diacetone alcohol	GC/MS, GC-FID	[105]
	Formic acid, acetic acid, mesityl oxide, diacetone alcohol	CIMS	[141]
MEK	Acetone, ethanol, acetaldehyde, acetic acid, methanol, formaldehyde, formic acid	GC/MS, GC-FID	[139]
Acetaldehyde	Formaldehyde, acetic acid	GC-FID, FTIR	[60]
	Acetic acid, formic acid, formaldehyde	FTIR	[128]
Ethanol	Acetaldehyde, formaldehyde, acetic acid, formic acid	GC-FID, FTIR	[60]
	Acetaldehyde, acetic acid, formaldehyde, formic acid	TPD-TPO	[131]
n-Butanol	n-Butanal, crotonaldehyde, propanal, acetaldehyde	GC-FID	[31]
	Butanal, butanoic acid, 1-propanol, propanal, ethanol, acetaldehyde	GC/MS	[133]

CIMS: Chemical ionization mass spectrometry; HPLC: High-performance liquid chromatography; FID: Flame ionization detector.
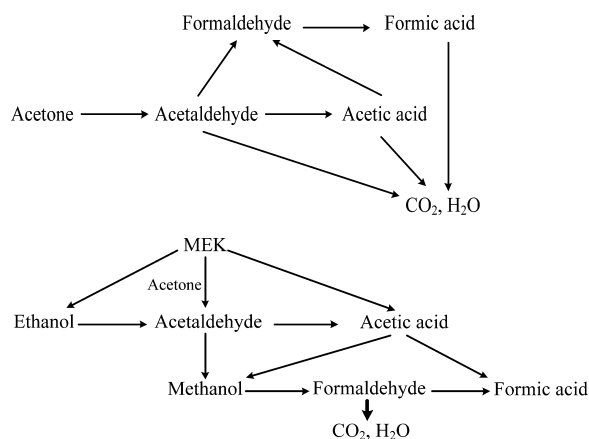
Fig. 8. Photocatalytic oxidation pathway of acetone [28] and MEK [139].

regeneration or replacement of the catalyst, which in turn increases the cost associated with the system [65,142–144]. Photocatalyst deactivation (i.e. loss of photocatalyst active sites) can stem from several sources: adsorption of reaction intermediates/by-products onto the photocatalyst surface (i.e. blockage of the active sites) [88,145], photo-polymerization of species on the surface [21,146], fouling and aggregation of TiO_2 nanoparticles [147], and deposition of SiO_2 onto the surface due to the presence of siloxane group materials in the environment [148]. Additionally, some studies [62,65,88] pointed out that the dehydroxylation of TiO_2 surface due to the consumption of hydroxyl radicals can remarkably reduce the lifetime of photocatalyst. This phenomenon can be effectively prevented by keeping the humidity content in the reactor high enough to continuously rehydrate the photocatalyst surface [63,65].

Taranto et al. [124] noticed a substantial decrement in methanol reaction rate over P25 immobilized on cellulose fibers at high I (108 W/m^2). They suggested due to the fact that cellulose is sensitive to UV irradiation, it is plausible that cellulose degradation products compete with methanol for the active species/sites, leading to lower reaction rate at high I. As mentioned earlier, adsorption of reaction intermediates on the surface is the most common source of photocatalyst deactivation; accordingly, several researchers have attempted to identify the adsorbed species on photocatalyst surface. To this end, using liquid phase acidic extraction technique, Thevenet et al. [121] identified formic, oxalic and acetic acids adsorbed on P25 surface during the PCO of acetylene and considered the adsorption of these carboxylic acids (either molecular or dissociative) as the main reason of photocatalyst deactivation. In another research, Einaga et al. [97] monitored the CO_x evolution during regeneration process of P25 employed in PCO of benzene, toluene, cyclohexane, and cyclohexene. They concluded that carbon deposits derived from aromatics were more resistant to oxidation compared to those from alkane and alkene. Diffuse reflectance infrared Fourier transform (DRIFT) spectra of P25 samples before and after PCO of toluene obviously revealed the presence of unreacted toluene (in huge amount), benzaldehyde and benzoic acid on the surface after 1000 min of operation, which totally impeded the oxidation reactions' progress [101]. It is worth mentioning that the adsorption of intermediates with hydrophilic features (e.g. acetone, acetic acid and benzaldehyde) on TiO_2 surface and/or the water film can greatly hamper the reaction of hydrophobic compounds [86,95,97]. Taking into account the presence of siloxanes in ambient air (at sub ppm levels), Hay and Obee [148] demonstrated that the irreversible deactivation of photocatalyst was the result of formation of an amorphous silica layer from photo-oxidation of siloxanes which blocks the pores of P25. Several studies have pointed out the importance of ozone-

generating lamps in order to elongate the lifetime of photocatalyst [49,83] owing to the high capability of ozone in decomposing carbon deposits and intermediates adsorbed on the surface. In this regard, Jeong et al. [83] investigated the long-term PCO of toluene and compared P25 deactivation under black light, germicidal, and ozone-generating lamps. At low concentration (0.6 ppm), no deactivation was noticed, whereas at higher concentration (4 ppm) and using black light/germicidal lamp, unlike ozone-generating lamp, photocatalyst activity was seriously suppressed after 400 min by deposition of benzaldehyde, benzyl alcohol, and benzoic acid on the surface. In marked contrast, some works have claimed the absence of any considerable photocatalyst deactivation [32,47,65,86]. For instance, Verbruggen et al. [47] stated that the steady state conversion of acetylene over P25 and PC500 did not show any noticeable decrement over 30 h of operation. Similarly, Taranto et al. [32] reported no dramatic decline in the steady state removal efficiency of methanol and n-octane over PC500, PC105, and P25 after 24 h of operation. In addition, Tsoukleris et al. [125] monitored the performance of P25 in PCO of some aromatics (ppm range) in 30 consecutive experiments spread over a 6-month period and no sign of activity loss was observed.

The common regeneration techniques include: exposing photocatalyst to dry or humidified air under UV light for long period of time [48,63,65,97,100,102,121], treating photocatalyst with a vaporized H_2O_2 solution and heating the surface to different temperatures [100,119], and ozone-purging in the presence of humidity [65,83,119]. By employing ozone in the regeneration process, Krichevskaya et al. [119] could significantly shorten the required time for restoration of P25 activity from hours of treatment (up to 15 h) with UVA at elevated temperatures (up to 180 °C) to 20 min using UVA + O_3. Piera et al. [100] examined a number of surface treatments in order to recover the activity of P25 used in PCO of ethanol. Exposure to UV irradiation, clean air (dry or humid), air containing H_2O_2, hot air flow (80–150 °C) or a combination of these processes for a long period of time (15–56 h) were investigated in this study.

In the literature, there are a number of works which were mainly focused on exploring one specific aspect of PCO in-depth. Some of these studies and their main focuses and findings are presented in Table 5.

6. Conclusion

In this review article, application of commercial photocatalysts for photocatalytic oxidation of indoor volatile organic compounds has been reviewed from various perspectives.

The interconnections between photocatalyst features such as crystallinity, surface area, and surface chemistry were further understood by analyzing the characterization results (e.g. SEM, XRD, TEM, XPS, FTIR and N_2 adsorption-desorption) and photocatalytic performance of different TiO_2 photocatalysts. It can be concluded that high crystallinity, small crystal size, co-presence of anatase and rutile, high surface area, porous structure, large amount of surface hydroxyl groups, and high photocatalyst surface density improve the photocatalytic activity. Furthermore, the advantageous effect of support materials such as activated carbon on VOC adsorption and removal efficiency were investigated. Despite extensive research on different photocatalysts for PCO, still there are plenty of unresolved issues required to be addressed thoroughly in order to enhance photocatalyst performance for a wide range of operating conditions and various VOCs.

The most influencing reaction parameters including airflow rate/residence time, VOC type and concentration, relative humidity, light source and light intensity were discussed in detail. In summary, there is good agreement among researchers regarding

Table 5
Selected articles on application of commercial photocatalysts in VOC photocatalytic degradation.

Compound	Focus	Remarks	Ref.
Toluene	Effect of RH	At very high RH, both low and high MW by-products are desorbed from the surface into the gas phase. At zero RH, by-products accumulate on the reaction surface and block the photocatalyst. At [Toluene] = 400 ppbv, higher PCO efficiency leads to lower concentrations of by-products in the gas phase. At [Toluene] = 800 ppbv, the maximum efficiency and minimum concentrations of by-products were obtained at different RHs.	[16]
Toluene	Deactivation and regeneration	Exposing the deactivated P25 to UV light for 2000 min under 70% RH completely recovered the photocatalytic activity. CO_2 selectivity was higher for the regenerated P25 due to the larger number of surface OH, evidenced by XPS, after regeneration under high RH.	[101]
Toluene	Short wavelength UV irradiation	Reactive oxygen species and hydroxyl radicals are of great importance when short WL UV light is used. Photocatalyst was completely deactivated after 120 min of operation, and regeneration (under 254 + 185 nm UV irradiation in humid air for 30 min) could completely recover the activity. Very high values (up to 90%) have been obtained for conversion of toluene due to the combination of photolysis, ozonation and OH radical attack in the absence of photocatalyst.	[49,83]
Toluene	Intermediates and reaction pathway	Based on VOC profiles, benzaldehyde, $o/m/p$-cresols can be regarded as toluene first reaction intermediates in the gas phase. Secondary intermediates are non-cyclic structures, such as aldehydes, resulting from aromatic ring-opening reactions. Working in humid condition increased CO_2 and decreased CO selectivity compared to experiments in dry air.	[111]
Acetylene	Deactivation and regeneration	Acetylene conversion and CO_2 selectivity dropped by 30% and 20% respectively only after 12 h of operation. Deactivation of the photocatalyst has been attributed to the irreversible adsorption of carboxylic acids on the surface.	[121]
Decane	Intermediates and reaction pathway	Ratios between intermediate concentration and decane concentration for formaldehyde and acetaldehyde, as the main reaction intermediates, considerably increased in humid conditions. Types and order of appearance of intermediates did not change noticeably, indicating the same reaction mechanism at different decane concentration.	[17]
Formaldehyde	Application of activated carbon	It has been shown that combination of netlike activated carbon and P25 can efficiently remove formaldehyde (removal rate up to 100%) in low concentrations and acceptable residence times. Depending on the concentration, behavior of removal efficiency and reaction rate against airflow rate vary. Netlike activated carbon by far outperformed granular activated carbon.	[72]
Acetaldehyde	Characteristics of P25 and PC500	It was revealed that more bulk recombination happens in PC500 in comparison to P25, which could arise from the presence of amorphous TiO_2 in PC500. Higher turnover frequency for PC500 was attributed to its higher surface area, surface hydroxyls, and adsorption properties.	[47]
Acetaldehyde	Intermediates and reaction pathway	Employing FTIR technique, it was noticed that acetaldehyde is bound to Aerolyst 7710 surface via its carbonyl group. Without illumination, when acetaldehyde is adsorbed on the surface, crotonaldehyde and 3-hydroxybutanal are formed via aldol condensation and bidentate acetate species are formed by an oxidation process.	[128]
n-butanol	Impact of thermal treatment	Calcination had a negligible effect on P25 surface area, adsorption capacity and efficiency, while it significantly decreased UV100 surface area and adsorption capacity. Under fluorescent white light the influence of photocatalyst crystallinity (P25 > UV100) on removal efficiency was less important compared to experiments under fluorescent black light.	[31]
Methanol, n-octane	Coating methods	In order to optimize the amount of TiO_2 deposited and the adhesion of the coating, seven parameters (e.g. dip coating suspension acidity, dip coating rate, number of coatings, and calcination temperature and time) was employed. It was showed that the number of coatings, suspension acidity and calcination temperature are the most influencing factors.	[32]
Methanol, Benzene	Effect of RH and concentration	Reaction rate constant diminished with increasing the concentration of methanol/benzene. Synergy coefficient (ratio of apparent rate constant for the mixture to that for single compound) was introduced to study the interaction between benzene and methanol. Based on the obtained values for synergy coefficient, presence of methanol has a positive influence on benzene PCO.	[64]
Formaldehyde, Toluene, 1,3-Butadiene	Effect of RH	Oxidation rate was improved by increasing the face velocity until it reaches its plateau where oxidation rate is freed from mass transfer and is controlled by surface reactions. In general, at very low humidity levels (below ca. 5000 ppmv) and high contaminant concentrations, a drop in oxidation rate with decreasing humidity levels was noticed. At high concentrations, increment in humidity content was always positive for toluene and negative for formaldehyde.	[62]
Various	Deactivation of photocatalyst by siloxanes	Based on XPS analysis, the extent of deactivation strongly depends on the amount of silica on the surface. Based on TEM images of deactivated P25, amorphous SiO_2 bridged the gap between crystallites and between the P25 agglomerate particles, and hindered the diffusion of gaseous species into interior regions. Installing an activated carbon filter prior to the PCO section to remove siloxanes could substantially suppress deactivation.	[148]

the impact of residence time, challenge compound concentration and light source intensity on PCO processes. Higher residence time, lower VOC concentration, higher light intensity and shorter light source wavelength favor the removal efficiency of pollutants and mineralization to CO_2. However, there is no general consensus regarding the effect of relative humidity, and depending on other operating factors, photocatalyst, and type of VOC, humidity can be promoting, inhibiting or both. It should be mentioned that most of the studies on PCO of VOCs were conducted under ideal operating conditions, especially in terms of residence time and VOC concentration. Consequently, more research is required to clarify the true potential of this technology under realistic conditions close to its actual application in buildings.

In the last two sections of the study, different reaction pathways and intermediates/by-products, the main sources of photocatalyst deactivation, and several regeneration techniques were reviewed. Nonetheless, there is limited knowledge available regarding the long-term performance of PCO system for application for indoor environment (real situation), by-products generation and associated health risks, deactivation mechanisms under different operating conditions and regeneration methods.

Applying the heretofore gained knowledge regarding the limitations of PCO technology for indoor air purification, a number of recommendations for future research can be put forward:

- Improving the morphological, electronic, and chemical characteristics of TiO_2 photocatalysts in order to enhance the photoactivity, adsorbability towards VOCs, and resistance to deactivation.
- Coupling the photocatalyst with suitable support material in order to suppress the adverse effect of humidity content on VOC removal efficiency.
- Evaluation of photocatalyst efficacy in real operating conditions including short residence times (ms range), low pollutant concentrations (ppb level), mixture of VOCs, and a wide range of relative humidity.
- Through understanding of possible reaction pathways for different VOCs in order to prevent the generation of strongly-adsorbed intermediates as well as harmful by-products by adjusting photocatalyst's features and/or operating parameters.
- Conducting long-term experiments (i.e. monitoring removal efficiency and mineralization degree over time) and exploring deactivation mechanisms and different regeneration methods.

Acknowledgements

References

[1] N.E. Klepeis, W.C. Nelson, W.R. Ott, J.P. Robinson, A.M. Tsang, P. Switzer, J.V. Behar, S.C. Hern, W.H. Engelmann, The national human activity pattern survey (NHAPS): a resource for assessing exposure to environmental pollutants, J. Expo. Anal. Environ. Epidemiol. 11 (2001) 231–252.

[2] L. Zhong, F. Haghighat, Photocatalytic air cleaners and materials technologies—abilities and limitations, Build. Environ. 91 (2015) 191–203.

[3] S. Wang, H.M. Ang, M.O. Tade, Volatile organic compounds in indoor environment and photocatalytic oxidation: state of the art, Environ. Int. 33 (2007) 694–705.

[4] S.W. Verbruggen, TiO2 photocatalysis for the degradation of pollutants in gas phase: from morphological design to plasmonic enhancement, J. Photochem. Photobiol. C: Photochem. Rev. 24 (2015) 64–82.

[5] F. Haghighat, C.-S. Lee, B. Pant, G. Bolourani, N. Lakdawala, A. Bastani, Evaluation of various activated carbons for air cleaning–towards design of immune and sustainable buildings, Atmos. Environ. 42 (2008) 8176–8184.

[6] A. Khazraei Vizhemehr, F. Haghighat, Modeling of gas-phase filter model for high- and low-challenge gas concentrations, Build. Environ. 80 (2014) 192–203.

[7] A. Shiue, Y.-H. Kang, S.-C. Hu, G.-T. Jou, C.-H. Lin, M.-C. Hu, S.-I. Lin, Vapor adsorption characteristics of toluene in an activated carbon adsorbent-loaded nonwoven fabric media for chemical filters applied to cleanrooms, Build. Environ. 45 (2010) 2123–2131.

[8] L. Zhong, C.-S. Lee, F. Haghighat, Adsorption performance of titanium dioxide (TiO2) coated air filters for volatile organic compounds, J. Hazard. Mater. 243 (2012) 340–349.

[9] Z. Fan, P. Lioy, C. Weschler, N. Fiedler, H. Kipen, J. Zhang, Ozone-initiated reactions with mixtures of volatile organic compounds under simulated indoor conditions, Environ. Sci. Technol. 37 (2003) 1811–1821.

[10] M.F. Boeniger, Use of ozone generating devices to improve indoor air quality, Am. Ind. Hyg. Assoc. J. 56 (1995) 590–598.

[11] L. Zhong, F. Haghighat, Ozonation air purification technology in HVAC applications, Ashrae Trans. 120 (2014).

[12] M. Bahri, F. Haghighat, S. Rohani, H. Kazemian, Impact of design parameters on the performance of non-thermal plasma air purification system, Chem. Eng. J. 302 (2016) 204–212.

[13] M. Bahri, F. Haghighat, Plasma-based indoor air cleaning technologies: the state of the art-review, Clean: Soil Air Water 42 (2014) 1667–1680.

[14] L. Zhong, F. Haghighat, C.-S. Lee, Ultraviolet photocatalytic oxidation for indoor environment applications: experimental validation of the model, Build. Environ. 62 (2013) 155–166.

[15] D. Farhanian, F. Haghighat, Photocatalytic oxidation air cleaner: identification and quantification of by-products, Build. Environ. 72 (2014) 34–43.

[16] J. Mo, Y. Zhang, Q. Xu, Effect of water vapor on the by-products and decomposition rate of ppb-level toluene by photocatalytic oxidation, Appl. Catal. B: Environ. 132–133 (2013) 212–218.

[17] O. Debono, F. Thévenet, P. Gravejat, V. Héquet, C. Raillard, L. Le Coq, N. Locoge, Gas phase photocatalytic oxidation of decane at ppb levels: removal kinetics, reaction intermediates and carbon mass balance, J. Photochem. Photobiol. A: Chem. 258 (2013) 17–29.

[18] H. Chen, C.E. Nanayakkara, V.H. Grassian, Titanium dioxide photocatalysis in atmospheric chemistry, Chem. Rev. 112 (2012) 5919–5948.

[19] K. Nakata, A. Fujishima, TiO2 photocatalysis: design and applications, J. Photochem. Photobiol. C: Photochem. Rev. 13 (2012) 169–189.

[20] J. Wen, X. Li, W. Liu, Y. Fang, J. Xie, Y. Xu, Photocatalysis fundamentals and surface modification of TiO2 nanomaterials, Chin. J. Catal. 36 (2015) 2049–2070.

[21] J. Mo, Y. Zhang, Q. Xu, Y. Zhu, J.J. Lamson, R. Zhao, Determination and risk assessment of by-products resulting from photocatalytic oxidation of toluene, Appl. Catal. B: Environ. 89 (2009) 570–576.

[22] A.A. Ismail, D.W. Bahnemann, Mesoporous titania photocatalysts: preparation, characterization and reaction mechanisms, J. Mater. Chem. 21 (2011) 11686–11707.

[23] B. Ohtani, O.O. Prieto-Mahaney, D. Li, R. Abe, What is Degussa (Evonik) P25? Crystalline composition analysis, reconstruction from isolated pure particles and photocatalytic activity test, J. Photochem. Photobiol. A: Chem. 216 (2010) 179–182.

[24] N. Bouazza, M.A. Lillo-Ródenas, A. Linares-Solano, Enhancement of the photocatalytic activity of pelletized TiO2 for the oxidation of propene at low concentration, Appl. Catal. B: Environ. 77 (2008) 284–293.

[25] T. Tytgat, B. Hauchecorne, A.M. Abakumov, M. Smits, S.W. Verbruggen, S. Lenaerts, Photocatalytic process optimisation for ethylene oxidation, Chem. Eng. J. 209 (2012) 494–500.

[26] A. Alonso-Tellez, R. Masson, D. Robert, N. Keller, V. Keller, Comparison of Hombikat UV100 and P25 TiO2 performance in gas-phase photocatalytic oxidation reactions, J. Photochem. Photobiol. A: Chem. 250 (2012) 58–65.

[27] A. Šuligoj, U.L. Štangar, A. Ristić, M. Mazaj, D. Verhovšek, N.N. Tušar, TiO2–SiO2 films from organic-free colloidal TiO2 anatase nanoparticles as photocatalyst for removal of volatile organic compounds from indoor air, Appl. Catal. B: Environ. 184 (2016) 119–131.

[28] C.L. Bianchi, S. Gatto, C. Pirola, A. Naldoni, A. Di Michele, G. Cerrato, V. Crocellà, V. Capucci, Photocatalytic degradation of acetone, acetaldehyde and toluene in gas-phase: comparison between nano and micro-sized TiO2, Appl. Catal. B: Environ. 146 (2014) 123–130.

[29] S.W. Verbruggen, S. Ribbens, T. Tytgat, B. Hauchecorne, M. Smits, V. Meynen, P. Cool, J.A. Martens, S. Lenaerts, The benefit of glass bead supports for efficient gas phase photocatalysis: case study of a commercial and a synthesised photocatalyst, Chem. Eng. J. 174 (2011) 318–325.

[30] M. Hajaghazadeh, V. Vaiano, D. Sannino, H. Kakooei, R. Sotudeh-Gharebagh, P. Ciambelli, Heterogeneous photocatalytic oxidation of methyl ethyl ketone under UV-A light in an LED-fluidized bed reactor, Catal. Today 230 (2014) 79–84.

[31] J. Kirchnerova, M.L. Herrera Cohen, C. Guy, D. Klvana, Photocatalytic oxidation of n-butanol under fluorescent visible light lamp over commercial TiO2 (Hombicat UV100 and Degussa P25), Appl. Catal. A: Gen. 282 (2005) 321–332.

[32] J. Taranto, D. Frochot, P. Pichat, Photocatalytic treatment of air: comparison of various TiO2, coating methods, and supports using methanol or n-octane as test pollutant, Ind. Eng. Chem. Res. 48 (2009) 6229–6236.

[33] V. Puddu, H. Choi, D.D. Dionysiou, G.L. Puma, TiO2 photocatalyst for indoor air remediation: influence of crystallinity, crystal phase, and UV radiation intensity on trichloroethylene degradation, Appl. Catal. B: Environ. 94 (2010) 211–218.

[34] A. Bazyari, A.A. Khodadadi, A. Haghighat Mamaghani, J. Beheshtian, L.T. Thompson, Y. Mortazavi, Microporous titania–silica nanocomposite catalyst-adsorbent for ultra-deep oxidative desulfurization, Appl. Catal. B: Environ. 180 (2016) 65–77.

[35] X. Li, J. Yu, M. Jaroniec, Hierarchical photocatalysts, Chem. Soc. Rev. 45 (2016) 2603–2636.

[36] A. Fujishima, X. Zhang, D.A. Tryk, TiO2 photocatalysis and related surface phenomena, Surf. Sci. Rep. 63 (2008) 515–582.

[37] R.A.R. Monteiro, S.M. Miranda, C. Rodrigues-Silva, J.L. Faria, A.M.T. Silva, R.A.R. Boaventura, V.J.P. Vilar, Gas phase oxidation of *n*-decane and PCE by photocatalysis using an annular photoreactor packed with a monolithic catalytic bed coated with P25 and PC500, Appl. Catal. B: Environ. 165 (2015) 306–315.

[38] D.C. Hurum, A.G. Agrios, K.A. Gray, T. Rajh, M.C. Thurnauer, Explaining the enhanced photocatalytic activity of degussa P25 mixed-phase TiO2 using EPR, J. Phys. Chem. B 107 (2003) 4545–4549.

[39] T. Ohno, K. Sarukawa, K. Tokieda, M. Matsumura, Morphology of a TiO2 photocatalyst (Degussa, P-25) consisting of anatase and rutile crystalline phases, J. Catal. 203 (2001) 82–86.

[40] R.I. Bickley, T. Gonzalez-Carreno, J.S. Lees, L. Palmisano, R.J.D. Tilley, A structural investigation of titanium dioxide photocatalysts, J. Solid State Chem. 92 (1991) 178–190.

[41] O. Tahiri Alaoui, A. Herissan, C. Le Quoc, M.E.M. Zekri, S. Sorgues, H. Remita, C. Colbeau-Justin, Elaboration, charge-carrier lifetimes and activity of Pd-TiO2 photocatalysts obtained by gamma radiolysis, J. Photochem. Photobiol. A: Chem. 242 (2012) 34–43.

[42] S.T. Martin, H. Herrmann, W. Choi, M.R. Hoffmann, Time-resolved microwave conductivity. Part 1.–TiO2 photoreactivity and size quantization, J. Chem. Soc. Faraday Trans. 90 (1994) 3315–3322.

[43] F. Thevenet, O. Guaïtella, J.M. Herrmann, A. Rousseau, C. Guillard, Photocatalytic degradation of acetylene over various titanium dioxide-based photocatalysts, Appl. Catal. B: Environ. 61 (2005) 58–68.

[44] Z. Zhang, C.-C. Wang, R. Zakaria, J.Y. Ying, Role of particle size in nanocrystalline TiO2-based photocatalysts, J. Phys. Chem. B 102 (1998) 10871–10878.

[45] T. van der Meulen, A. Mattson, L. Österlund, A comparative study of the photocatalytic oxidation of propane on anatase, rutile, and mixed-phase anatase–rutile TiO2 nanoparticles: role of surface intermediates, J. Catal. 251 (2007) 131–144.

[46] J. Araña, A.P. Alonso, J.M.D. Rodríguez, G. Colón, J.A. Navío, J.P. Peña, FTIR study of photocatalytic degradation of 2-propanol in gas phase with different TiO2 catalysts, Appl. Catal. B: Environ. 89 (2009) 204–213.

[47] S.W. Verbruggen, K. Masschaele, E. Moortgat, T.E. Korany, B. Hauchecorne, J.A. Martens, S. Lenaerts, Factors driving the activity of commercial titanium dioxide powders towards gas phase photocatalytic oxidation of acetaldehyde, Catal. Sci. Technol. 2 (2012) 2311–2318.

[48] O. d'Hennezel, P. Pichat, D.F. Ollis, Benzene and toluene gas-phase photocatalytic degradation over H2O and HCL pretreated TiO2: by-products and mechanisms, J. Photochem. Photobiol. A: Chem. 118 (1998) 197–204.

[49] J. Jeong, K. Sekiguchi, W. Lee, K. Sakamoto, Photodegradation of gaseous volatile organic compounds (VOCs) using TiO2 photoirradiated by an ozone-producing UV lamp: decomposition characteristics, identification of by-products and water-soluble organic intermediates, J. Photochem. Photobiol. A: Chem. 169 (2005) 279–287.

[50] J.C. Yu, J. Lin, D. Lo, S.K. Lam, Influence of thermal treatment on the adsorption of oxygen and photocatalytic activity of TiO2, Langmuir 16 (2000) 7304–7308.

[51] M. Jafarikojour, M. Sohrabi, S.J. Royaee, A. Hassanvand, Evaluation and optimization of a novel immobilized photoreactor for the degradation of gaseous toluene, Clean Soil Air Water 43 (2015) 662–670.

[52] N. Quici, M.L. Vera, H. Choi, G.L. Puma, D.D. Dionysiou, M.I. Litter, H. Destaillats, Effect of key parameters on the photocatalytic oxidation of toluene at low concentrations in air under 254 + 185 nm UV irradiation, Appl. Catal. B: Environ. 95 (2010) 312–319.

[53] C. Guillard, D. Debayle, A. Gagnaire, H. Jaffrezic, J.-M. Herrmann, Physical properties and photocatalytic efficiencies of TiO2 films prepared by PECVD and sol–gel methods, Mater. Res. Bull. 39 (2004) 1445–1458.

[54] A.H. Aïssa, E. Puzenat, A. Plassais, J.-M. Herrmann, C. Haehnel, C. Guillard, Characterization and photocatalytic performance in air of cementitious materials containing TiO2. Case study of formaldehyde removal, Appl. Catal. B: Environ. 107 (2011) 1–8.

[55] H. Einaga, T. Ibusuki, S. Futamura, Photocatalytic oxidation of benzene in air, J. Solar Energy Eng. 126 (2004) 789–793.

[56] D. Vildozo, C. Ferronato, M. Sleiman, J.-M. Chovelon, Photocatalytic treatment of indoor air: optimization of 2-propanol removal using a response surface methodology (RSM), Appl. Catal. B: Environ. 94 (2010) 303–310.

[57] W.A. Jacoby, D.M. Blake, R.D. Noble, C.A. Koval, Kinetics of the oxidation of trichloroethylene in air via heterogeneous photocatalysis, J. Catal. 157 (1995) 87–96.

[58] R.A.R. Monteiro, A.M.T. Silva, J.R.M. Ângelo, G.V. Silva, A.M. Mendes, R.A.R. Boaventura, V.J.P. Vilar, Photocatalytic oxidation of gaseous perchloroethylene over TiO2 based paint, J. Photochem. Photobiol. A: Chem. 311 (2015) 41–52.

[59] W. Choi, J.Y. Ko, H. Park, J.S. Chung, Investigation on TiO2-coated optical fibers for gas-phase photocatalytic oxidation of acetone, Appl. Catal. B: Environ. 31 (2001) 209–220.

[60] M.R. Nimlos, E.J. Wolfrum, M.L. Brewer, J.A. Fennell, G. Bintner, Gas-phase heterogeneous photocatalytic oxidation of ethanol: pathways and kinetic modeling, Environ. Sci. Technol. 30 (1996) 3102–3110.

[61] A.K. Boulamanti, C.J. Philippopoulos, Photocatalytic degradation of C5–C7 alkanes in the gas–phase, Atmos. Environ. 43 (2009) 3168–3174.

[62] T.N. Obee, R.T. Brown, TiO2 photocatalysis for indoor air applications: effects of humidity and trace contaminant levels on the oxidation rates of formaldehyde, toluene, and 1,3-butadiene, Environ. Sci. Technol. 29 (1995) 1223–1231.

[63] A.K. Boulamanti, C.A. Korologos, C.J. Philippopoulos, The rate of photocatalytic oxidation of aromatic volatile organic compounds in the gas-phase, Atmos. Environ. 42 (2008) 7844–7850.

[64] G. Qijin, W. Qingming, Z. Bin, Adsorption and photocatalytic oxidation of methanol–benzene binary mixture in an annular fluidized bed photocatalytic reactor, Ind. Eng. Chem. Res. 51 (2012) 15360–15373.

[65] R.M. Alberici, W.F. Jardim, Photocatalytic destruction of VOCs in the gas-phase using titanium dioxide, Appl. Catal. B: Environ. 14 (1997) 55–68.

[66] D. Vildozo, R. Portela, C. Ferronato, J.-M. Chovelon, Photocatalytic oxidation of 2-propanol/toluene binary mixtures at indoor air concentration levels, Appl. Catal. B: Environ. 107 (2011) 347–354.

[67] K.-P. Yu, G.W.M. Lee, W.-M. Huang, C. Wu, S. Yang, The correlation between photocatalytic oxidation performance and chemical/physical properties of indoor volatile organic compounds, Atmos. Environ. 40 (2006) 375–385.

[68] Q. Geng, Q. Guo, X. Yue, Adsorption and photocatalytic degradation kinetics of gaseous cyclohexane in an annular fluidized bed photocatalytic reactor, Ind. Eng. Chem. Res. 49 (2010) 4644–4652.

[69] L. Zhang, W.A. Anderson, S. Sawell, C. Moralejo, Mechanistic analysis on the influence of humidity on photocatalytic decomposition of gas-phase chlorobenzene, Chemosphere 68 (2007) 546–553.

[70] D. Kibanova, M. Sleiman, J. Cervini-Silva, H. Destaillats, Adsorption and photocatalytic oxidation of formaldehyde on a clay-TiO2 composite, J. Hazard. Mater. 211–212 (2012) 233–239.

[71] M.A. Lillo-Ródenas, N. Bouazza, A. Berenguer-Murcia, J.J. Linares-Salinas, P. Soto, A. Linares-Solano, Photocatalytic oxidation of propene at low concentration, Appl. Catal. B: Environ. 71 (2007) 298–309.

[72] Y. Lu, D. Wang, C. Ma, H. Yang, The effect of activated carbon adsorption on the photocatalytic removal of formaldehyde, Build. Environ. 45 (2010) 615–621.

[73] C.H. Ao, S.C. Lee, Combination effect of activated carbon with TiO2 for the photodegradation of binary pollutants at typical indoor air level, J. Photochem. Photobiol. A: Chem. 161 (2004) 131–140.

[74] W.-K. Jo, C.-H. Yang, Granular-activated carbon adsorption followed by annular-type photocatalytic system for control of indoor aromatic compounds, Sep. Purif. Technol. 66 (2009) 438–442.

[75] J. Araña, J.M. Doña-Rodríguez, E. Tello Rendón, C. Garriga i Cabo, O. González-Díaz, J.A. Herrera-Melián, J. Pérez-Peña, G. Colón, J.A. Navío, TiO2 activation by using activated carbon as a support: part II. Photoreactivity and FTIR study, Appl. Catal. B: Environ. 44 (2003) 153–160.

[76] W. Den, C.-C. Wang, Enhancement of adsorptive chemical filters via titania photocatalysts to remove vapor-phase toluene and isopropanol, Sep. Purif. Technol. 85 (2012) 101–111.

[77] C.H. Ao, S.C. Lee, Enhancement effect of TiO2 immobilized on activated carbon filter for the photodegradation of pollutants at typical indoor air level, Appl. Catal. B: Environ. 44 (2003) 191–205.

[78] S. Nagaoka, Y. Hamasaki, S.-I. Ishihara, M. Nagata, K. Iio, C. Nagasawa, H. Ihara, Preparation of carbon/TiO2 microsphere composites from cellulose/TiO2 microsphere composites and their evaluation, J. Mol. Catal. A: Chem. 177 (2002) 255–263.

[79] N. Bouazza, M.A. Lillo-Ródenas, A. Linares-Solano, Photocatalytic activity of TiO2-based materials for the oxidation of propene and benzene at low concentration in presence of humidity, Appl. Catal. B: Environ. 84 (2008) 691–698.

[80] H. Yoneyama, T. Torimoto, Titanium dioxide/adsorbent hybrid photocatalysts for photodestruction of organic substances of dilute concentrations, Catal. Today 58 (2000) 133–140.

[81] J. Mo, Y. Zhang, Q. Xu, R. Yang, Effect of TiO2/adsorbent hybrid photocatalysts for toluene decomposition in gas phase, J. Hazard. Mater. 168 (2009) 276–281.

[82] C.H. Ao, S.C. Lee, Indoor air purification by photocatalyst TiO2 immobilized on an activated carbon filter installed in an air cleaner, Chem. Eng. Sci. 60 (2005) 103–109.

[83] J. Jeong, K. Sekiguchi, K. Sakamoto, Photochemical and photocatalytic degradation of gaseous toluene using short-wavelength UV irradiation with TiO2 catalyst: comparison of three UV sources, Chemosphere 57 (2004) 663–671.

[84] D. Farhanian, F. Haghighat, C.-S. Lee, N. Lakdawala, Impact of design parameters on the performance of ultraviolet photocatalytic oxidation air cleaner, Build. Environ. 66 (2013) 148–157.

[85] G. Vincent, P.M. Marquaire, O. Zahraa, Photocatalytic degradation of gaseous 1-propanol using an annular reactor: kinetic modelling and pathways, J. Hazard. Mater. 161 (2009) 1173–1181.

[86] M. Sleiman, P. Conchon, C. Ferronato, J.-M. Chovelon, Photocatalytic oxidation of toluene at indoor air levels (ppbv): towards a better assessment

of conversion, reaction intermediates and mineralization, Appl. Catal. B: Environ. 86 (2009) 159–165.

[87] A. Bouzaza, C. Vallet, A. Laplanche, Photocatalytic degradation of some VOCs in the gas phase using an annular flow reactor: determination of the contribution of mass transfer and chemical reaction steps in the photodegradation process, J. Photochem. Photobiol. A: Chem. 177 (2006) 212–217.

[88] L. Cao, F.-J. Spiess, A. Huang, S.L. Suib, T.N. Obee, S.O. Hay, J.D. Freihaut, Heterogeneous photocatalytic oxidation of 1-butene on SnO$_2$ and TiO$_2$ films, J. Phys. Chem. B 103 (1999) 2912–2917.

[89] P.-A. Deveau, F. Arsac, P.-X. Thivel, C. Ferronato, F. Delpech, J.-M. Chovelon, P. Kaluzny, C. Monnet, Different methods in TiO$_2$ photodegradation mechanism studies: gaseous and TiO$_2$-adsorbed phases, J. Hazard. Mater. 144 (2007) 692–697.

[90] F.V.S. Lopes, R.A.R. Monteiro, A.M.T. Silva, G.V. Silva, J.L. Faria, A.M. Mendes, V.J.P. Vilar, R.A.R. Boaventura, Insights into UV-TiO$_2$ photocatalytic degradation of PCE for air decontamination systems, Chem. Eng. J. 204–206 (2012) 244–257.

[91] N. Djeghri, M. Formenti, F. Juillet, S.J. Teichner, Photointeraction on the surface of titanium dioxide between oxygen and alkanes, Faraday Discuss. Chem. Soc. 58 (1974) 185–193.

[92] O. d'Hennezel, D.F. Ollis, Trichloroethylene-promoted photocatalytic oxidation of air contaminants, J. Catal. 167 (1997) 118–126.

[93] W. Wang, Y. Ku, Photocatalytic degradation of gaseous benzene in air streams by using an optical fiber photoreactor, J. Photochem. Photobiol. A: Chem. 159 (2003) 47–59.

[94] T.N. Obee, S.O. Hay, Effects of moisture and temperature on the photooxidation of ethylene on titania, Environ. Sci. Technol. 31 (1997) 2034–2038.

[95] F. Tang, X. Yang, A deactivation kinetic model for predicting the performance of photocatalytic degradation of indoor toluene, o-xylene, and benzene, Build. Environ. 56 (2012) 329–334.

[96] P. Pichat, Some views about indoor air photocatalytic treatment using TiO$_2$: conceptualization of humidity effects active oxygen species, problem of C1–C3 carbonyl pollutants, Appl. Catal. B: Environ. 99 (2010) 428–434.

[97] H. Einaga, S. Futamura, T. Ibusuki, Heterogeneous photocatalytic oxidation of benzene, toluene, cyclohexene and cyclohexane in humidified air: comparison of decomposition behavior on photoirradiated TiO$_2$ catalyst, Appl. Catal. B: Environ. 38 (2002) 215–225.

[98] K.-P. Yu, G.W.-M. Lee, W.-M. Huang, C.-C. Wu, C.-L. Lou, S. Yang, Effectiveness of photocatalytic filter for removing volatile organic compounds in the heating, ventilation, and air conditioning system, J. Air Waste Manage. Assoc. 56 (2006) 666–674.

[99] T. Guo, Z. Bai, C. Wu, T. Zhu, Influence of relative humidity on the photocatalytic oxidation (PCO) of toluene by TiO$_2$ loaded on activated carbon fibers: PCO rate and intermediates accumulation, Appl. Catal. B: Environ. 79 (2008) 171–178.

[100] E. Piera, J.A. Ayllón, X. Doménech, J. Peral, TiO$_2$ deactivation during gas-phase photocatalytic oxidation of ethanol, Catal. Today 76 (2002) 259–270.

[101] M.-G. Jeong, E.J. Park, H.O. Seo, K.-D. Kim, Y.D. Kim, D.C. Lim, Humidity effect on photocatalytic activity of TiO$_2$ and regeneration of deactivated photocatalysts, Appl. Surf. Sci. 271 (2013) 164–170.

[102] T.N. Obee, Photooxidation of sub-parts-per-million toluene and formaldehyde levels on titania using a glass-plate reactor, Environ. Sci. Technol. 30 (1996) 3578–3584.

[103] N. Doucet, O. Zahraa, M. Bouchy, Kinetics of the photocatalytic degradation of benzene, Catal. Today 122 (2007) 168–177.

[104] D. Kibanova, J. Cervini-Silva, H. Destaillats, Efficiency of clay – TiO$_2$ nanocomposites on the photocatalytic elimination of a model hydrophobic air pollutant, Environ. Sci. Technol. 43 (2009) 1500–1506.

[105] G. Vincent, P.M. Marquaire, O. Zahraa, Abatement of volatile organic compounds using an annular photocatalytic reactor: study of gaseous acetone, J. Photochem. Photobiol. A: Chem. 197 (2008) 177–189.

[106] W.-K. Jo, J.-H. Park, H.-D. Chun, Photocatalytic destruction of VOCs for in-vehicle air cleaning, J. Photochem. Photobiol. A: Chem. 148 (2002) 109–119.

[107] C.H. Ao, S.C. Lee, J.Z. Yu, J.H. Xu, Photodegradation of formaldehyde by photocatalyst TiO$_2$: effects on the presences of NO, SO2 and VOCs, Appl. Catal. B: Environ. 54 (2004) 41–50.

[108] Y. Luo, D.F. Ollis, Heterogeneous photocatalytic oxidation of trichloroethylene and toluene mixtures in air: kinetic promotion and inhibition time-dependent catalyst activity, J. Catal. 163 (1996) 1–11.

[109] C.-P. Chang, J.-N. Chen, M.-C. Lu, Heterogeneous photocatalytic oxidation of acetone for air purification by near UV-irradiated titanium dioxide, J. Environ. Sci. Health: A 38 (2003) 1131–1143.

[110] H. Einaga, S. Futamura, T. Ibusuki, Photocatalytic decomposition of benzene over TiO$_2$ in a humidified airstream, Phys. Chem. Chem. Phys. 1 (1999) 4903–4908.

[111] O. Debono, F. Thevenet, P. Gravejat, V. Hequet, C. Raillard, L. Lecoq, N. Locoge, Toluene photocatalytic oxidation at ppbv levels: kinetic investigation and carbon balance determination, Appl. Catal. B: Environ. 106 (2011) 600–608.

[112] F. Thevenet, O. Guaitella, E. Puzenat, C. Guillard, A. Rousseau, Influence of water vapour on plasma/photocatalytic oxidation efficiency of acetylene, Appl. Catal. B: Environ. 84 (2008) 813–820.

[113] D.H. Chen, X. Ye, K. Li, Oxidation of PCE with a UV LED photocatalytic reactor, Chem. Eng. Technol. 28 (2005) 95–97.

[114] J.-M. Herrmann, Heterogeneous photocatalysis: fundamentals and applications to the removal of various types of aqueous pollutants, Catal. Today 53 (1999) 115–129.

[115] S.B. Kim, S.C. Hong, Kinetic study for photocatalytic degradation of volatile organic compounds in air using thin film TiO$_2$ photocatalyst, Appl. Catal. B: Environ. 35 (2002) 305–315.

[116] Z. Pengyi, L. Fuyan, Y. Gang, C. Qing, Z. Wanpeng, A comparative study on decomposition of gaseous toluene by O$_3$/UV, TiO$_2$/UV and O$_3$/TiO$_2$/UV, J. Photochem. Photobiol. A: Chem. 156 (2003) 189–194.

[117] S. Toby, L.J. Van de Burgt, F.S. Toby, Kinetics and chemiluminescence of ozone-aromatic reactions in the gas phase, J. Phys. Chem. 89 (1985) 1982–1986.

[118] P. Pichat, J. Disdier, C. Hoang-Van, D. Mas, G. Goutailler, C. Gaysse, Purification/deodorization of indoor air and gaseous effluents by TiO$_2$ photocatalysis, Catal. Today 63 (2000) 363–369.

[119] M. Krichevskaya, S. Preis, A. Moiseev, N. Pronina, J. Deubener, Gas-phase photocatalytic oxidation of refractory VOCs mixtures: through the net of process limitations, Catal. Today (2016), http://dx.doi.org/10.1016/j.cattod.2016.03.041.

[120] J.L. Coutts, L.H. Levine, J.T. Richards, D.W. Mazyck, The effect of photon source on heterogeneous photocatalytic oxidation of ethanol by a silica–titania composite, J. Photochem. Photobiol. A: Chem. 225 (2011) 58–64.

[121] F. Thevenet, C. Guillard, A. Rousseau, Acetylene photocatalytic oxidation using continuous flow reactor: gas phase and adsorbed phase investigation assessment of the photocatalyst deactivation, Chem. Eng. J. 244 (2014) 50–58.

[122] Y. Tao, C.-Y. Wu, D.W. Mazyck, Removal of methanol from pulp and paper mills using combined activated carbon adsorption and photocatalytic regeneration, Chemosphere 65 (2006) 35–42.

[123] W.-K. Jo, K.-H. Park, Heterogeneous photocatalysis of aromatic and chlorinated volatile organic compounds (VOCs) for non-occupational indoor air application, Chemosphere 57 (2004) 555–565.

[124] J. Taranto, D. Frochot, P. Pichat, Photocatalytic air purification: comparative efficacy and pressure drop of a TiO2-coated thin mesh and a honeycomb monolith at high air velocities using a 0.4 m^3 close-loop reactor, Sep. Purif. Technol. 67 (2009) 187–193.

[125] D.S. Tsoukleris, T. Maggos, C. Vassilakos, P. Falaras, Photocatalytic degradation of volatile organics on TiO$_2$ embedded glass spherules, Catal. Today 129 (2007) 96–101.

[126] Y.-P. Zhang, R. Yang, Q.-J. Xu, J.-H. Mo, Characteristics of photocatalytic oxidation of toluene, benzene, and their mixture, J. Air Waste Manage. Assoc. 57 (2007) 94–101.

[127] D. Cazoir, D. Vildozo, M. Sleiman, C. Ferronato, L. Fine, J.-M. Chovelon, Analysis of gas phase intermediates and mineralization during the photocatalytic oxidation of organic pollutants: a critical step towards the performance evaluation, Int. J. Environ. Anal. Chem. 92 (2012) 923–932.

[128] B. Hauchecorne, D. Terrens, S. Verbruggen, J.A. Martens, H. Van Langenhove, K. Demeestere, S. Lenaerts, Elucidating the photocatalytic degradation pathway of acetaldehyde: an FTIR in situ study under atmospheric conditions, Appl. Catal. B: Environ. 106 (2011) 630–638.

[129] S. Kim, S.K. Lim, Preparation of TiO$_2$-embedded carbon nanofibers and their photocatalytic activity in the oxidation of gaseous acetaldehyde, Appl. Catal. B: Environ. 84 (2008) 16–20.

[130] H. Ibrahim, H. de Lasa, Photo-catalytic conversion of air borne pollutants: effect of catalyst type and catalyst loading in a novel photo-CREC-air unit, Appl. Catal. B: Environ. 38 (2002) 201–213.

[131] D.S. Muggli, J.T. McCue, J.L. Falconer, Mechanism of the photocatalytic oxidation of ethanol on TiO$_2$, J. Catal. 173 (1998) 470–483.

[132] M.L. Sauer, D.F. Ollis, Photocatalyzed oxidation of ethanol and acetaldehyde in humidified air, J. Catal. 158 (1996) 570–582.

[133] F. Benoit-Marquié, U. Wilkenhöner, V. Simon, A.M. Braun, E. Oliveros, M.-T. Maurette, VOC photodegradation at the gas–solid interface of a TiO2 photocatalyst: part I: 1-butanol and 1-butylamine, J. Photochem. Photobiol. A: Chem. 132 (2000) 225–232.

[134] J. Peral, D.F. Ollis, Heterogeneous photocatalytic oxidation of gas-phase organics for air purification: acetone, 1-butanol, butyraldehyde, formaldehyde, and m-xylene oxidation, J. Catal. 136 (1992) 554–565.

[135] N.R. Blake, G.L. Griffin, Selectivity control during the photoassisted oxidation of 1-butanol on titanium dioxide, J. Phys. Chem. 92 (1988) 5697–5701.

[136] S.A. Larson, J.L. Falconer, Initial reaction steps in photocatalytic oxidation of aromatics, Catal. Lett. 44 (1997) 57–65.

[137] T.J. Frankcombe, S.C. Smith, OH-initiated oxidation of toluene. 1. Quantum chemistry investigation of the reaction path, J. Phys. Chem. A 111 (2007) 3686–3690.

[138] X. Ye, D. Chen, J. Gossage, K. Li, Photocatalytic oxidation of aldehydes: byproduct identification and reaction pathway, J. Photochem. Photobiol. A: Chem. 183 (2006) 35–40.

[139] C. Raillard, V. Héquet, P. Le Cloirec, J. Legrand, Photocatalytic oxidation of methyl ethyl ketone over sol-gel and commercial TiO$_2$ for the improvement of indoor air, Water Sci. Technol. 53 (2006) 107–115.

[140] A.L. Attwood, J.L. Edwards, C.C. Rowlands, D.M. Murphy, Identification of a surface alkylperoxy radical in the photocatalytic oxidation of acetone/O$_2$ over TiO$_2$, J. Phys. Chem. A 107 (2003) 1779–1782.

[141] C.M. Schmidt, A.M. Buchbinder, E. Weitz, F.M. Geiger, Photochemistry of the indoor air pollutant acetone on degussa P25 TiO$_2$ studied by chemical ionization mass spectrometry, J. Phys. Chem. A 111 (2007) 13023–13031.

[142] A.H. Mamaghani, B. Najafi, A. Casalegno, F. Rinaldi, Long-term economic analysis and optimization of an HT-PEM fuel cell based micro combined heat and power plant, Appl. Therm. Eng. 99 (2016) 1201–1211.

[143] B. Najafi, A.H. Mamaghani, F. Rinaldi, A. Casalegno, Long-term performance analysis of an HT-PEM fuel cell based micro-CHP system: operational strategies, Appl. Energy 147 (2015) 582–592.

[144] A. Haghighat Mamaghani, B. Najafi, A. Casalegno, F. Rinaldi, Predictive modelling and adaptive long-term performance optimization of an HT-PEM fuel cell based micro combined heat and power (CHP) plant, Appl. Energy (2016), http://dx.doi.org/10.1016/j.apenergy.2016.08.050.

[145] S. Ardizzone, C.L. Bianchi, G. Cappelletti, A. Naldoni, C. Pirola, Photocatalytic degradation of toluene in the gas phase: relationship between surface species and catalyst features, Environ. Sci. Technol. 42 (2008) 6671–6676.

[146] M.L. Sauer, D.F. Ollis, Catalyst deactivation in gas–solid photocatalysis, J. Catal. 163 (1996) 215–217.

[147] J. Zhao, X. Yang, Photocatalytic oxidation for indoor air purification: a literature review, Build. Environ. 38 (2003) 645–654.

[148] S.O. Hay, T.N. Obee, C. Thibaud-Erkey, The deactivation of photocatalytic based air purifiers by ambient siloxanes, Appl. Catal. B: Environ. 99 (2010) 435–441.